

COMPARISON OF ELECTRON CYCLOTRON RESONANCE  
DRY ETCH CHEMISTRIES FOR SILICON CARBIDE

BY  
GAVIN McDANIEL

A THESIS PRESENTED TO THE GRADUATE SCHOOL  
OF THE UNIVERSITY OF FLORIDA IN PARTIAL FULFILLMENT  
OF THE REQUIREMENTS FOR THE DEGREE OF  
MASTER OF SCIENCE

UNIVERSITY OF FLORIDA

1997

19970613 014

REPORT DOCUMENTATION PAGE			Form Approved OMB No. 0704-0188	
Public reporting burden for this collection of information is estimated to average 1 hour per response, including the time for reviewing instructions, searching existing data sources, gathering and maintaining the data needed, and completing and reviewing the collection of information. Send comments regarding this burden estimate or any other aspect of this collection of information, including suggestions for reducing this burden, to Washington Headquarters Services, Directorate for Information Operations and Reports, 1215 Jefferson Davis Highway, Suite 1204, Arlington, VA 22202-4302, and to the Office of Management and Budget, Paperwork Reduction Project (0704-0188), Washington, DC 20503.				
1. AGENCY USE ONLY (Leave blank)		2. REPORT DATE 3 JUN 97		3. REPORT TYPE AND DATES COVERED
4. TITLE AND SUBTITLE COMPARISON OF ELECTRON CYCLTRON RESONANCE DRY ETCH CHEMISTRIES FOR SILICON CARBIDE			5. FUNDING NUMBERS	
6. AUTHOR(S) GAVIN Y. MCDANIEL				
7. PERFORMING ORGANIZATION NAME(S) AND ADDRESS(ES) GRDUATE SCHOOL OF THE UNIVERSITY OF FLORIDA			8. PERFORMING ORGANIZATION REPORT NUMBER  97-055	
9. SPONSORING/MONITORING AGENCY NAME(S) AND ADDRESS(ES) DEPARTMENT OF THE AIR FORCE AFIT/CI 2950 P STREET WRIGHT-PATTERSON AFB OH 45433-7765			10. SPONSORING/MONITORING AGENCY REPORT NUMBER	
11. SUPPLEMENTARY NOTES				
12a. DISTRIBUTION AVAILABILITY STATEMENT  <div style="border: 1px solid black; padding: 5px; text-align: center;"> <b>DISTRIBUTION STATEMENT A</b>            Approved for public release            Distribution Unlimited         </div>			12b. DISTRIBUTION CODE	
13. ABSTRACT (Maximum 200 words)				
14. SUBJECT TERMS			15. NUMBER OF PAGES 76	
			16. PRICE CODE	
17. SECURITY CLASSIFICATION OF REPORT	18. SECURITY CLASSIFICATION OF THIS PAGE	19. SECURITY CLASSIFICATION OF ABSTRACT	20. LIMITATION OF ABSTRACT	

COMPARISON OF ELECTRON CYCLOTRON RESONANCE  
DRY ETCH CHEMISTRIES FOR SILICON CARBIDE

BY  
GAVIN McDANIEL

A THESIS PRESENTED TO THE GRADUATE SCHOOL  
OF THE UNIVERSITY OF FLORIDA IN PARTIAL FULFILLMENT  
OF THE REQUIREMENTS FOR THE DEGREE OF  
MASTER OF SCIENCE

UNIVERSITY OF FLORIDA

1997

## ACKNOWLEDGMENTS

I would like to express my sincerest gratitude to Dr. Paul H. Holloway and Dr. Stephen Pearton who took me under their wings. Dr. Holloway worked with me long before I arrived at the University of Florida and actively took an interest in my preparation and achievement of goals with the Air Force while I have been at UF. As my co-advisors, they have given me countless hours of instruction and guidance for which I am grateful. I would also like to thank committee members, Dr. Rolf Hummel and Dr. Gijs Bosman. Each of the members of my committee has been available for discussion and has given me direction throughout this study without hesitation. They have been vital to the completion of my work.

I would like to express my appreciation for the patience and instruction given to me by Jewon Lee as he taught me how to run the Plasma Therm for etching and the Dektak for analysis. Jewon taught me a lot about etching theory and was a motivational mentor and I thank him for that. Jacques Cuno deserves a lot of credit for teaching me how to use the AFM. He always helped me fine tune my techniques and he could always be counted on for advice when the "ghost" in the machine would make characterization difficult. I owe Eric Lambers my thanks for characterizing my samples with the Auger electron spectrometer. He always provided the time and patience to explain techniques to me and I could always count on him for a smile. I would like to thank The Department of Defense for allocating funds to the Air Force for research assistantships through the Air

Force Institute of Technology (AFIT). My two year education has been funded by one of these assistantships. I'd like to thank ONR and the University of Florida for funding the research and providing equipment and materials. I'd also like to thank Dr. Fau Ren from Bell Laboratories for providing 3C-SiC for the research.

Finally, I would like to thank my family, Wyatt, Sandy, and Gardner and my friends for keeping me motivated when times were difficult. They have been my strength many times.

## TABLE OF CONTENTS

ACKNOWLEDGMENTS.....	ii
LIST OF TABLES.....	vi
LIST OF FIGURES.....	viii
ABSTRACT.....	xi
CHAPTERS	
1. INTRODUCTION.....	1
1.1 Background.....	1
1.2 SiC Characteristics.....	1
1.3 Dry Etching of SiC.....	5
1.4 Reactive Ion Etching (RIE).....	7
1.5 High Density Plasmas.....	13
1.6 Theory of Reactive Ion Etching.....	14
2. EXPERIMENTAL PROCEDURES.....	21
2.1 Samples.....	21
2.2 Etching Conditions.....	23
2.3 Characterization.....	24
2.3.1 Stylus Profilometry.....	24
2.3.2 Atomic Force Microscopy (AFM).....	25
2.3.3 Auger Electron Spectroscopy (AES).....	26
3. RESULTS AND DISCUSSION.....	28
3.1 Etch Rate.....	28
3.1.1 Etch Rate Results.....	28
3.1.2 Etch Rate Discussion.....	33
3.1.2.1 Dependence on ECR Power.....	33
3.1.2.2 Dependence on RF Power.....	37
3.1.2.3 Dependence on Total Pressure.....	40
3.1.2.4 Dependence on Flow Rate.....	41
3.2 AFM.....	42
3.2.1 Results.....	44
3.2.2 Discussion.....	46
3.3 AES.....	48
3.3.1 AES Results.....	48

3.3.2 AES Discussion.....	50
3.3.2.1 Argon etches.....	50
3.3.2.2 Sulfur hexafluoride etches.....	51
3.3.2.3 Iodine bromide etches.....	53
3.3.2.4 Chlorine etches.....	54
4. CONCLUSIONS.....	56
APPENDIX A: AFM IMAGES.....	60
APPENDIX B: PSD CURVES.....	70
LIST OF REFERENCES.....	74
BIOGRAPHICAL SKETCH.....	76

## LIST OF TABLES

<u>Table</u>	<u>Page</u>
1	Comparison of Properties for GaN, Diamond, Si, GaAs, and SiC.....2
2	Range of experimental conditions studied using 3C-SiC. (* - indicates where 6H-SiC was used in addition to 3C-SiC for analysis of surface morphology and surface composition).....23
3	Etch rate in Å/min as a function of ECR Power for a total pressure of mTorr, 150 Watts RF power, and constant flow rate ratio. (* indicates the ratio of active to total flow rates for that gas chemistry) .....28
4	Etch rate in Å/min as a function of RF power for a total pressure of 1.5 mTorr, 1000 Watts ECR power, and constant flow rate ratio. (* indicates the ratio of active to total flow rates for that gas chemistry). Table 5. Etch rate as a function of chamber pressure.....30
5	Etch rate in Å/min as a function of plasma chamber pressure for 150 Watts RF power, 1000 Watts ECR power, and constant flow rate ratio. (* indicates the ratio of active to total flow rates for that gas chemistry).....31
6	Etch rate in Å/min as a function of active to total flow rate ratios for 150 Watts RF power, 1000 Watts ECR power, and for a total pressure of 1.5 mTorr.....32
7	Estimation of sputter yield using the mass comparison relationship between the incident ions and the sputtered species, carbon and silicon.....34
8	Volatilities of several expected etch products for SF <sub>6</sub> /Ar chemistries. Free energy of formation for all species indicate that they will spontaneously form.....52
9	Volatility of the expected etch product for IBr/Ar chemistries. Free energy of formation indicates that this species will not spontaneously form.....53
10	Volatilities of several expected etch products for Cl <sub>2</sub> /Ar and Cl <sub>2</sub> /H <sub>2</sub> SF <sub>6</sub> /Ar



chemistries. Free energy of formation for all species except silane indicate  
that they will spontaneously form. Silane will not.....54

## LIST OF FIGURES

Figure	Page
1	View of atomic arrangement for a) zincblende 3C-SiC, b) wurtzite 2H-SiC, c) 4H-SiC, and d) 6H-SiC for the (111) and (0001) surfaces perpendicular to the plane of the page. The arrangement is shown such that each Si-C pair is located within the same plane, however, each pair is either above or below the plane of its adjacent nearest neighboring pairs.....4
2	SiC bandgap as a function of the fraction of hexagonal bonding.....5
3	Diagram of Electron Cyclotron Resonance Plasma Therm model 770 dry etching system.....7
4	Various processes possible for an electron interacting with a gas versus electron energy.....10
5	Voltage distribution as a function of alternating RF bias.....11
6	Sputter dependence on ion energy.....12
7	Comparison of pure chemical and pure sputter etching.....16
8	General example of the dependence of etch rate on a variable such as RF power, ECR power, pressure, or gas flow ratios over the full range of that variable.....18
9	Schematic of the procedure used to determine etch rate.....25
10	AFM cantilever motion and the resulting information for a single trace in the x-direction. Multiple scans along the x-axis are made as the tip moves along the y-axis to result in a two dimensional image of the surface topography.....26
11	Electron energy level representations of A) valence band ionization, B) core level ionization and photon emission, and C) core level ionization and auger emission as a result of electron impact on chlorine.....27

12	Etch rate in Å/min as a function of ECR Power for a total pressure of 1.5 mTorr, 150 Watts RF power, and constant flow rate ratio.....	29
13	Etch rate in Å/min as a function of RF power for a total pressure of 1.5 mTorr, 1000 Watts ECR power, and constant flow rate ratio.....	30
14	Etch rate in Å/min as a function of plasma chamber pressure for 150 Watts RF power, 1000 Watts ECR power, and constant flow rate ratio....	31
15a	Etch rate in Å/min as a function of active to total flow rate ratios for 150 Watts RF power, 1000 Watts ECR power, and for a total pressure of 1.5 mTorr for Cl <sub>2</sub> /Ar.....	32
15b	Etch rate in Å/min as a function of active to total flow rate ratios for 150 Watts RF power, 1000 Watts ECR power, and for a total pressure of 1.5 mTorr for IBr/Ar .....	33
16	Calculated theoretical etch rates as a function of RF power compared to measured etch rates.....	39
17	Procedure for determining RMS roughness for a given sample. Two 10 x 10 µm scans were obtained for each sample. Three to four 1 x 1 µm sections were chosen from each scan where scratches were minimal. RMS roughness calculations were performed on each of these regions and averaged to get the RMS average roughness for the given sample...	43
18	Representative PSD curves comparing roughness for Cl <sub>2</sub> /H <sub>2</sub> plasmas with varying ECR power.....	44
19	Average RMS roughness trends for a) Ar with variable RF power b) SF <sub>6</sub> /Ar for variable RF power c) IBr/Ar for variable flow rate of IBr d) Cl <sub>2</sub> /H <sub>2</sub> for variable ECR power. The dotted lines represent the RMS roughness of the unetched parent sample.....	45
20	AES depth profiles for argon plasmas with 1000 Watts ECR power, 1.5 mTorr total pressure, 15 sccm flow rate, and a) 50 Watts RF power b) 350 Watts RF Power.....	48
21	AES Depth profiles for sulfur hexafluoride plasmas with 1000 Watts ECR power, 1.5 mTorr total pressure, 0.667 active flow rate to total flow rate ratio, and a) 50 Watts RF power b) 250 Watts RF Power.....	49
22	AES Depth profiles for iodine bromide plasmas with 1000 Watts ECR power, 1.5 mTorr total pressure, 150 Watts RF power and a) 0.5 active flow rate to total flow rate ratio and b) Pure IBr at a flow rate of 8 sccm..	49

23	AES Depth profiles for chlorine plasmas with 1000 Watts ECR power, 1.5 mTorr total pressure, 0.667 active flow rate to total flow rate ratio, 150 Watts RF power, and a) argon as the carrier gas and b) hydrogen as the carrier gas.....	50
24	AES depth profile for the parent, unetched control sample indicating the carbon depleted and silicon terminated surface.....	51
25	Portion of the theoretical etch rate curve that each gas chemistry belongs to under the range of conditions studied. The etch rate ranges are shown in Å/min for each chemistry. The axis for the theoretical curve is EP as shown in Figure 8.....	57

Abstract of Thesis Presented to the Graduate School  
of the University of Florida in Partial Fulfillment of the  
Requirements for the Degree of Master of Science

COMPARISON OF ELECTRON CYCLOTRON RESONANCE  
DRY ETCH CHEMISTRIES FOR SILICON CARBIDE

By

Gavin Y. McDaniel

May 1997

Chairman: Dr. Paul H. Holloway

Major Department: Materials Science and Engineering

Plasma etching using an electron cyclotron resonance (ECR) source has been used to study dry etching of SiC. Gas chemistries studied include  $\text{Cl}_2/\text{Ar}$ ,  $\text{Cl}_2/\text{H}_2$ ,  $\text{SF}_6/\text{Ar}$ ,  $\text{IBr}/\text{Ar}$ , and Ar. The variables studied include ECR power (400 to 1000 W), RF power (50 to 350 W), chamber pressure (1.5 to 10 mTorr), and active to total gas flow rate ratios (0 to 1). Etch rates in excess of 2000 Å/min. have been achieved with  $\text{SF}_6/\text{Ar}$  ECR discharges at low power (400 Watts) and moderate RF power (100-150 Watts). The rates for  $\text{Cl}_2/\text{Ar}$  are comparable to  $\text{SF}_6/\text{Ar}$  rates with those for  $\text{Cl}_2/\text{H}_2$  being somewhat lower.  $\text{IBr}/\text{Ar}$  is found to be a very poor chemistry for SiC with etch rates reaching only 1000 Å/min. Pure Ar sputtering achieved rates of less than 800 Å/min. Smooth surfaces (0.6-0.8 nm RMS roughness) have been achieved in all plasma chemistries with no dependence of roughness on plasma conditions. Auger electron analysis confirmed carbon enrichment of the surface in most cases. High RF biases resulted in stoichiometric termination of the SiC surface. Silicon depletion was noted for low RF biases and high chlorine content plasmas. Contamination by F and S was noted in  $\text{SF}_6/\text{Ar}$  discharges. All gas chemistries studied favored the chemically dominant side of the theoretical etch rate curve with the

exception of pure argon, which favored the sputter dominant side. Chlorine showed the most synergistic effects and covered the largest range of the theoretical etch rate curve for the experimental conditions studied.

## CHAPTER 1 INTRODUCTION

### 1.1 Background

The discovery of high temperature semiconductor device technology has prompted studies of growth, characterization, and application of the III-V nitrides, II-VI compound semiconductors and column IV compound semiconductors such as SiC. The first two materials are more optically oriented. SiC's intrinsic properties have made it the subject of microelectronics studies in harsh environments, which is a concern for avionics research. The Wright Patterson AFB Materials Directorate is currently investigating MBE growth of SiC. To complement this research, an investigation of dry etching steps in device fabrication with SiC was pursued at the University of Florida.

### 1.2 SiC Characteristics

Until recently, semiconductor microelectronics studies focused mainly on Si and GaAs. These semiconductors, while useful, are limited to operations near room temperature with low current. Excess temperatures and high current densities cause the devices to fail. This, combined with the search for blue and green photon emitting devices, has led to the development of wide band gap semiconductors. SiC is one of these materials. Though emission of blue light is noteworthy, SiC's indirect bandgap limits its efficiency in optoelectronic applications. In the optoelectronics industry, SiC is being used

more as a substrate for GaN because of close lattice matching. Its intrinsic electronic properties, however, show a dominance over other semiconductors for microelectronics devices.<sup>1, 2, 3, 4</sup>

Table 1. Comparison of Properties for GaN, Diamond, Si, GaAs, and SiC.<sup>1</sup>

Property	GaN	Diamond	Si	GaAs	3C SiC	6H SiC
Band Gap (eV)	3.39	5.5	1.1	1.4	2.2	2.9
Maximum Temperature (K)	Ukn	1400	600	760	1200	1580
Melting Point (K)	1773	4273	1690	1510	Sublimes >2100	Sublimes >2100
Physical Stability	Good	Excellent	Good	Fair	Excellent	Excellent
Electron Mobility (cm <sup>2</sup> /V*s)	900	2200	1400	8500	1000	600
Hole Mobility (cm <sup>2</sup> /V*s)	150	1600	600	400	40	90
Breakdown Voltage (10 <sup>6</sup> V/cm <sup>2</sup> )	5	10	0.3	0.4	4	Ukn
Thermal Conductivity (W/cm)	1.3	20	1.5	0.5	5	4.9

SiC has many advantages over Si and GaAs. Its directional covalent bonds make it useful in mechanical applications with high stress, such as aircraft hydraulics and heat radiators for satellites.<sup>1</sup> With a Mohs Hardness of 9, it is second only to diamond for durability.<sup>4</sup> Also important in electronics applications is the mobility of carriers in the semiconductor. This limits the “speed” of the device. Data in Table 1 shows SiC’s electron mobility rivals GaN and is comparable to Si. In addition, the large bandgap allows for larger biases and greater power without production of excess carriers and recombinations leading to thermal and electrical breakdown. With SiC’s large bandgap



and stability at temperatures lower than 2100 K, devices using this material should be easily capable of operating over the range of 600-1000 C.<sup>5</sup> In addition to the high sublimation temperature, SiC's very high thermal conductivity aids in device cooling. This result of covalent bonds and low phonon interaction is similar to the high thermal conductivity of diamond. The high electron mobility also results from this effect.

Directional covalent bonds are responsible for many of SiC's properties. Si and C are both period IV elements. They require four electrons to satisfy their valence shells and achieve a full octet noble gas configuration. To do this, Si bonds to three C atoms and vice versa, such that the lattice consists of a tetrahedral bilayer. The fourth bond for both Si and C is used to attach atoms of one bilayer to another. Thus polytypes result from variations in stacking of the bilayers. There are three conventional placements, designated A, B, C, for a bilayer lattice. A lattice which is periodic (---ABCABC---) is purely zincblende (cubic), while one with a stacking sequence (---ABABA---) is purely hexagonal wurtzite. Figure 1 a) and b) shows pure cubic 3C-SiC ( $\beta$ -SiC) and hexagonal 2H-SiC ( $\alpha$ -SiC) structures of SiC. The bilayers run perpendicular and into the page. Polytypes exist in any number of combinations of the two structures shown above. The most commonly studied forms of SiC are the 6H and 4H polytypes and 3C. 4H is 50% cubic and 50% hexagonal in nearest neighbor bonding, while 6H is 2/3 cubic 1/3 hexagonal as shown in Figure 1 c).<sup>1</sup>

Each of these close packed systems has distinguishable characteristics, but the most notable effect is on the bandgap and electronic properties. The bandgap changes nonlinearly from 2.2 to 3.3 eV as the fraction of hexagonal nearest neighbor bonding increases (Figure 2). Bandgap engineering may therefore be used by varying the fraction

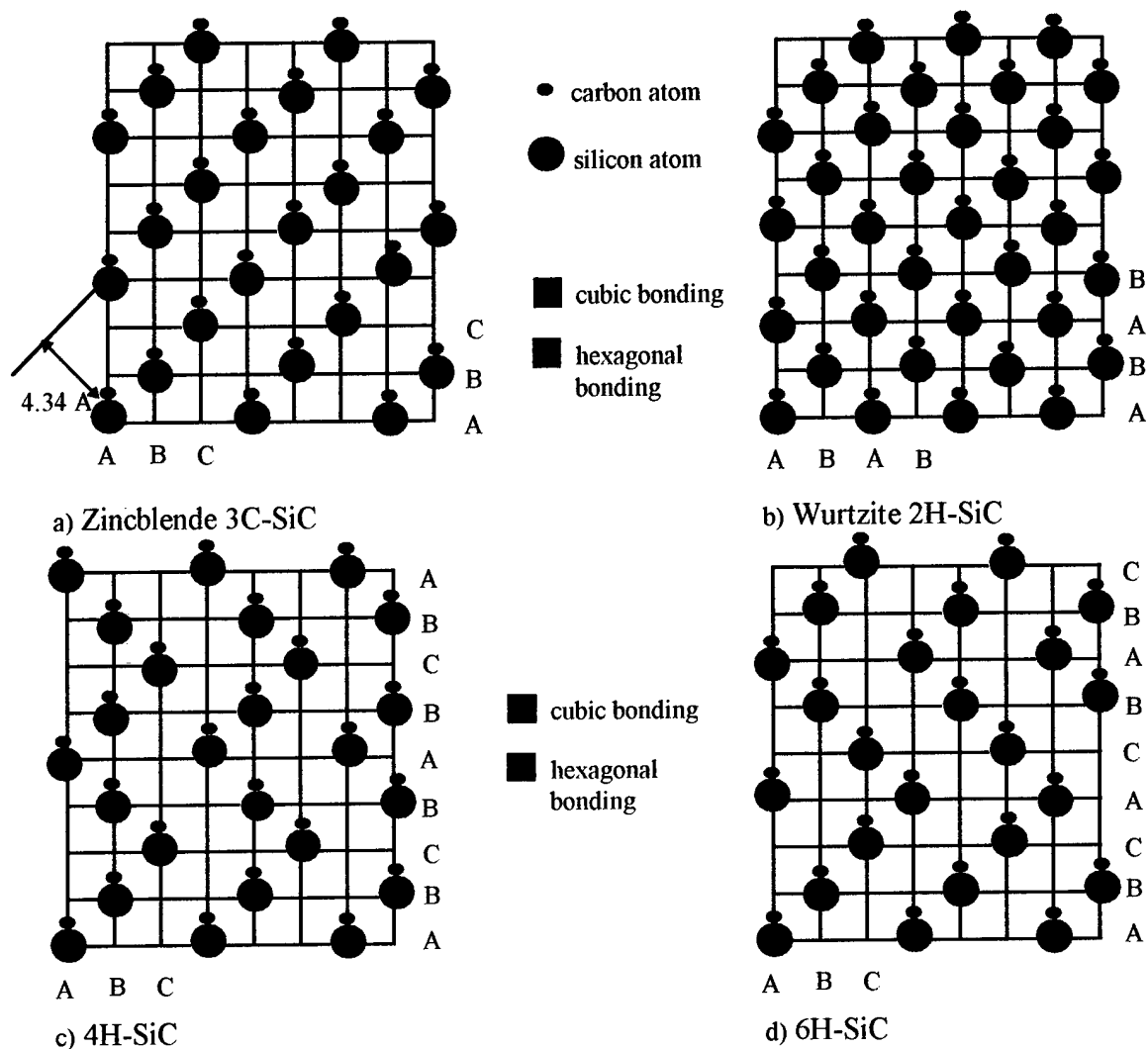


Figure 1. View of atomic arrangement for a) zincblende 3C-SiC, b) wurtzite 2H-SiC, c) 4H-SiC, and d) 6H-SiC for the (111) and (0001) surfaces perpendicular to the plane of the page. The arrangement is shown such that each Si-C pair is located within the same plane, however, each pair is either above or below the plane of its adjacent nearest neighboring pairs.<sup>1</sup>

of the wurtzite component. Although the bandgap increases, some electronic properties may suffer from increased hexagonal concentrations. For example, Morkoc *et al.*<sup>1</sup> report that 3C-SiC has the highest electron mobility and saturation velocity [versus polytypes] because of reduced phonon scattering resulting from its higher symmetry. This is surprising considering that Moki *et al.*<sup>6</sup> report that 3C-SiC on Si substrates has the highest defect concentration of all polytypes because of a 20% lattice mismatch. Clearly

the ability to control the bandgap and electronic properties is an additional advantage of SiC over Si or GaN for microelectronics devices. Though there may be advantageous properties for a given polytype, its ease of fabrication must be considered. The most

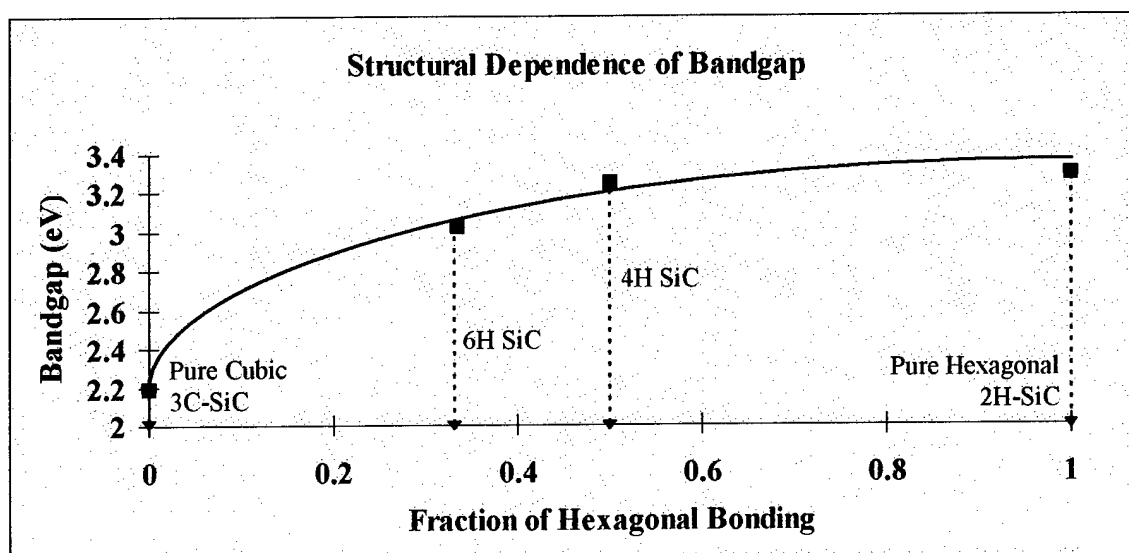


Figure 2. SiC bandgap as a function of the fraction of hexagonal bonding.

easily prepared of the polytypes is 6H, although 4H polytype and 3C seem to have better electrical characteristics and are the focus of recent studies. Developments in growth technology will help in this problem.

### 1.3 Dry Etching of SiC

Wet etching has been the conventional method for patterning semiconductors.<sup>7</sup> The surface is patterned with a nonreactive mask of photoresist or polymer and acid or base applied to the surface. Exposed sections react to form etch products that are soluble and are easily removed. This type of processing usually results in highly isotropic reaction rates and sloping sidewalls with severe undercutting, resulting in poor definition of small

features. Since many semiconductors are compounds, different species may be preferentially etched and structural orientation may affect the etching process.<sup>7</sup>

Dry etching avoids many of the problems associated with wet etching by combining chemical reactions with sputtering from heavy positive ions.<sup>7</sup> Some advantages of dry etching over wet etching include anisotropy control, less limitations on feature size because there is no surface tension or wettability effects, and less waste products.<sup>7</sup> Feature sizes are limited in wet etching by the rate of undercutting during etching. In ideal dry etching, there is no undercut and the integrity of the mask can be maintained. Thus features can be much smaller with more device fabrication. Dry etching has not replaced wet etching entirely since patterning of devices often requires both techniques.

To use SiC for a microelectronics or optoelectronics device, the fabrication process will involve patterning steps. Wu and Parsons<sup>8</sup> have reported etching of SiC by molten salts, gas reactions, electrolysis and by photochemistry techniques. Because SiC is very chemically stable, conventional wet etching is often unsatisfactory.<sup>9</sup> SiC is simply too resistant to most acids and other liquid etchants.<sup>10</sup> The strength of the covalent bond between Si and C makes reaction kinetics very slow at the surface. Diffusion of the wet etchant into small dimension volumes is slow which reduces its effectiveness. Silicon may also be passivated by exposure to air, forming highly protective layers of  $\text{SiO}_2$  which are known for their resistance to chemical attack. All of these characteristics combine to limit wet etching for SiC patterning. Dry etching is a reasonable alternative.

### 1.4 Reactive Ion Etching (RIE)

A diagram of a typical high density plasma system is shown in Figure 3. The sample to be etched is placed at the base of an evacuated chamber on an electrode. Typically two gases are supplied to the chamber at constant flow rates and constant

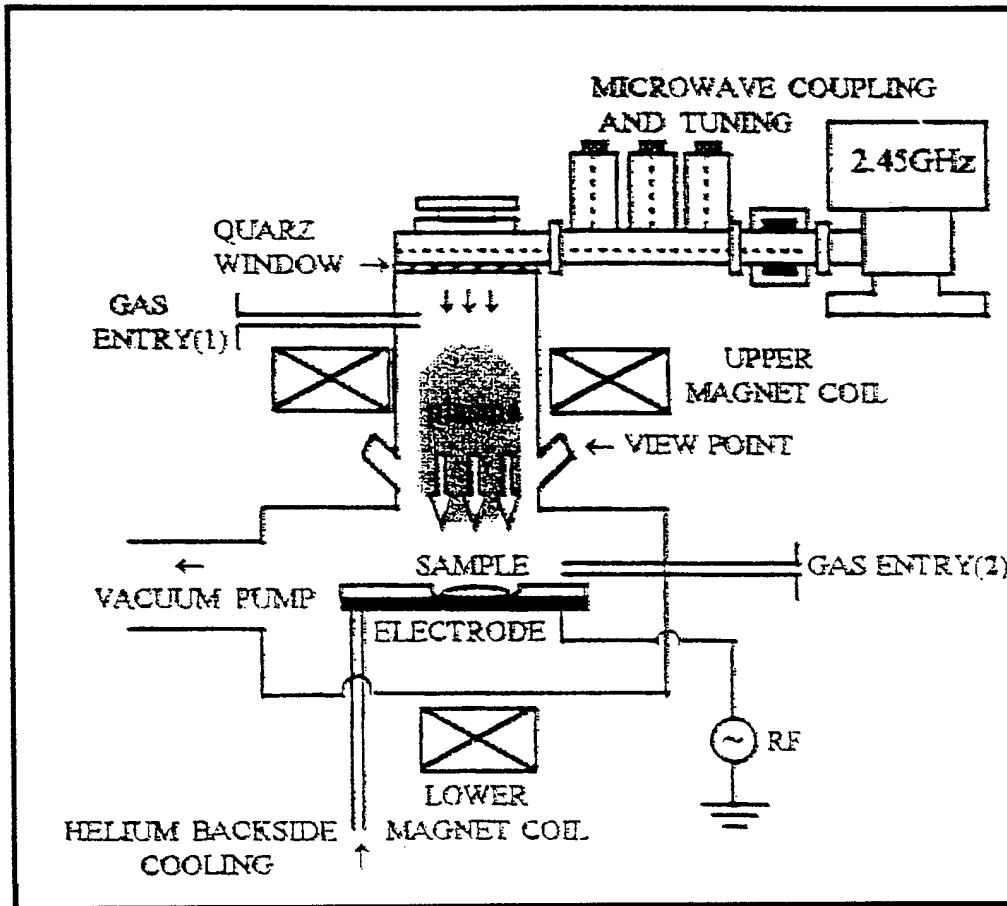


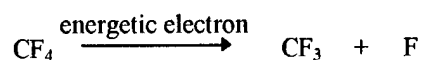
Figure 3. Diagram of Electron Cyclotron Resonance Plasma Therm model 770 dry etching system.<sup>11</sup>

flow rate ratios. A carrier gas is usually chosen as a nonreactive noble gas such as argon or a less reactive gas such as molecular hydrogen. The second gas usually contains a highly reactive component, often a halide. A voltage-driven current creates a plasma from the gases which is constrained by a magnetic field above the sample. A net negative bias

develops on the sample electrode from the RF bias due to the higher mobility of electrons versus positive ions. The negative bias attracts positive ions from the plasma toward the sample surface with energies sufficiently large to cause sputtering. The majority of the positive ions are from the noble carrier gas. Ion sputtering occurs uniformly across the surface with perpendicular impact trajectories. In addition to the sputtering, chemical reactions take place at the surface between neutral reactive gas atoms, reactive molecules, and radicals. These chemical reactions result in volatile etch products that undergo sputter-enhanced removal from the surface.<sup>7</sup> The total etching process is a combination of the chemical reactions plus sputter removal.

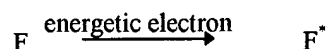
Several parameters control the etching process, one being the nature of the plasma. Electron collisions with neutral gases can cause dissociation, excitation, or ionization.<sup>12</sup> Electrons are impact-removed from both the active chemical species as well as the noble carrier gas. Charge neutrality of the plasma is always maintained between the number of ions and electrons. The electrons' high mobility allows them to respond to the alternating fields by moving quickly in the direction of the electric field within the plasma.

Dissociation of parent molecules is the primary mechanism for liberating highly reactive submolecular and atomic species. For example,  $\text{CF}_4$  is a strong fluorine donor when the molecule has been dissociated in the plasma. The dissociation follows the mechanism given below.<sup>12</sup>



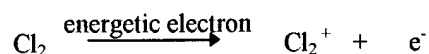
Continued dissociation of  $\text{CF}_3$  will liberate more fluorine radicals.

Excitation occurs when kinetic energy is transferred from the free electron to bound electrons in the molecules. The transferred energy promotes the bound electrons to higher energy states of the neutral atoms as shown below.<sup>12</sup>



The “glow” of the plasma is evidence of these excitations. When the electrons return to their ground states, light is given off which can be analyzed to identify the species that were activated. The energy released by de-excitation has also been hypothesized to overcome any activation energy barriers for reactions on the sample surface. However, this hypothesis has yet to be confirmed.

Electron impact excitation and ionization are the primary sources for both excited neutrals and ions. Ions are important since sputter-removal of the reaction products formed on the surface by radicals and activated neutrals lead to synergistic effects. Ionization can also occur by electron capture to form negative ions, however these are repelled from the sample and are not part of the etch process. They are not considered in this research. The process for making positive ions involves transfer of kinetic energy from the free electrons to a bound electron in the plasma gases. This process is shown below.<sup>12</sup>



The plasma's effectiveness in etching a sample will depend on the degree to which each of the above processes take place. A high ion density will enhance sputter etching of the sample, while a high density of free radicals and activated neutrals will enhance

chemical reaction of the surface. The energy of the electrons will dictate which process dominates as shown in figure 4. Note that all processes will occur within the plasma

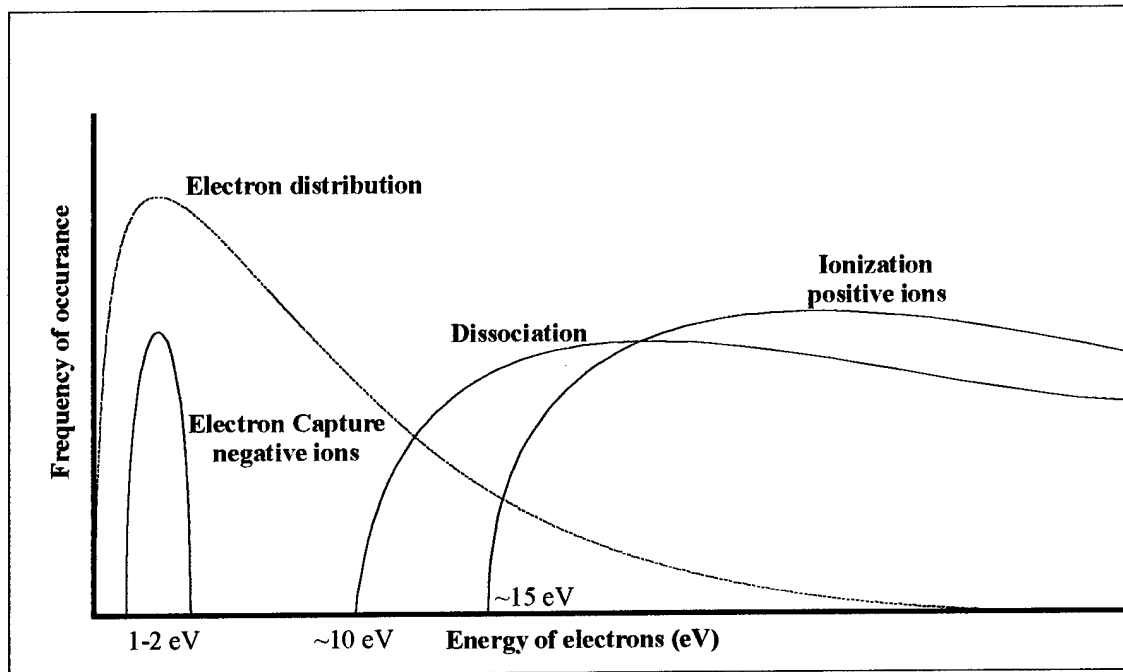


Figure 4. Various processes possible for an electron interacting with a gas versus electron energy.<sup>12</sup>

because the electrons will have a distribution of energies due to random collisions and varying pathlengths. The maximum energy is set by the maximum voltage applied (typically 100-300 eV), and will range down to a value below which ionization or excitation will not occur (approximately 1-2 eV).

The behavior of the plasma constituents must be known to understand the RIE process. There is no reason for directional movement of any species within the plasma except for ions under the influence of a voltage. Thus neutrals and reactive radicals will etch the surface only if they diffuse to the surface and react. Because the gas pressure is in the range of milliTorr where molecular mean free paths are large, it is likely that ions will strike the surface and lead to etching.



One of the requirements of the plasma is charge flux neutrality. With an RF bias, the higher mobility of electrons will allow them to reach insulated surfaces, such as the wall, the sample, and the sample electrode, more quickly than positive ions. The electron current will initially be high until the surfaces become negatively charged. The electron flux to the surfaces will be reduced due to the lower electric field, while the positive ion flux will be increased. Eventually the flux of electrons will be reduced so that it is equal to the ion flux. Under this condition, charge neutrality will be maintained and there will be no net current.<sup>12</sup> This negative charge buildup will create a negative dc self bias on the sample. The repulsion of electrons and acceleration of positive ions by this negative potential creates a sheath region which is indicated by a "dark space" above the sample. Electrons will not enter the sheath region so no activation of plasma species is possible and electron/positive ion recombinations will not take place. Thus, no light is emitted in this area. Positive ions randomly moving in the plasma see this bias as a potential well and

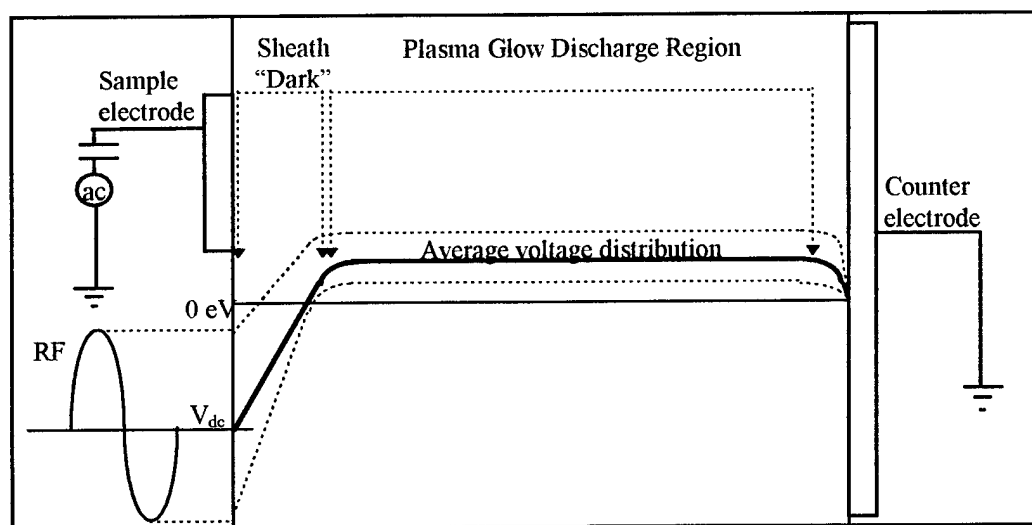


Figure 5. Voltage distribution as a function of alternating RF bias.<sup>12</sup>

will accelerate toward the surface if they drift into the sheath region. Figure 5 demonstrates this phenomenon. Asymmetric electrodes and a magnetically confined plasma prevent this from occurring in large amounts anywhere other than at the sample electrode.

Clearly ions will impinge the surface with a range of energies whose maximum is set by the supply voltage and the self bias potential which develops. Increasing the voltage will increase the energy of the impinging ions. Ions may be simple atoms or molecules consisting of 2 or more atoms. In the sputtering process, each atom within a molecular ion upon impact acts as though it has dissociated and the kinetic energy of the parent ion will be divided amongst the species in order to conserve energy and momentum. The following figure and example demonstrates this important relationship. In Figure 6,  $A^+$  represents one constituent in any molecular ion with positive one charge. Consider the following four ions:  $A^+$ ,  $A_2^+$ ,  $A_4^+$ , and  $A^{2+}$ . If an accelerating voltage of 100 volts was

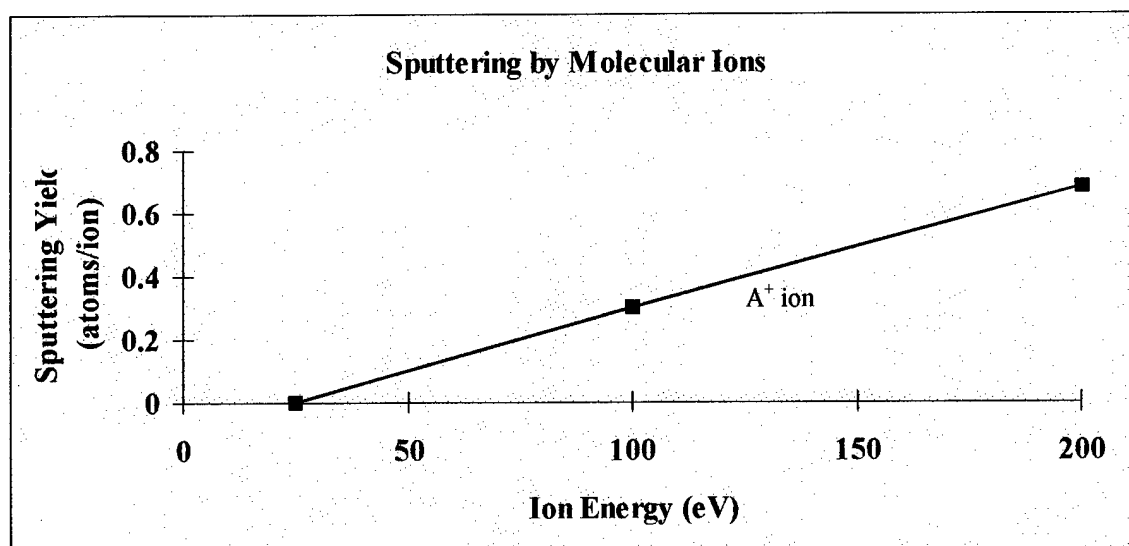


Figure 6. Sputter dependence on ion energy.<sup>12</sup>

applied to the sample, the  $A^+$  ion will have a sputter yield of 0.3 atoms/ion. The  $A_2^+$  ion will have a sputter yield of only 0.2 because each constituent has only 50 volts of energy

and thus contributes .1 to the sputtering yield. For the same reason the  $A_4^+$  ion will have 0 sputtering yield since the fragment energy would be only 25 eV which is below the sputter threshold of 25 eV. The doubly ionized single atom will have a sputtering yield of 0.7, which is greater than two of the singly ionized species.<sup>12</sup> Clearly the plasma ionization and dissociation will have a large effect on the extent of sputter etching.

The last variable in the etching process to be discussed is the pressure of gases in the chamber. The gases are introduced into an evacuated chamber raising the chamber pressure to the order of milliTorrs. The lower the pressure, the lower the concentration of all species. This can have two effects. The total number of reactive radicals and neutrals will be lower at low pressures. Thus both the chemical reactions and sputter rates will be reduced. The lower numbers of particles in the system will also reduce the probability of collisions between particles so the mean free path of ions will be increased. This will increase the sputter etching flux. The molecular mean free path in cm varies roughly as  $5/\text{pressure (mT)}$ .<sup>12</sup> This path length depends on the species in the plasma gases and is only used as an estimate.

### 1.5 High Density Plasmas

All the theory presented thus far is true for most RIE processes. Recently the density of plasmas has been increased. Electron cyclotron resonance (ECR) is one technique by which this may be accomplished. In this process, electrons that are used for excitation of the plasma are accelerated by magnetic fields in circular directions in the plasma region. The electron trajectories are controlled by the magnetic field lines and will respond to quickly changing field directions. A resonance is established which allows the

electrons to reach high velocities before colliding with gas molecules because pressures are kept low (mTorr) in the chamber. Independent control of the magnets allows the user to increase the density of the plasma active species and ions to several orders of magnitude higher than in normal RIE systems.<sup>12</sup>

Increased plasma density has several advantages. Most notably, there are more active species available for etching and more ions for sputtering. With higher densities, lower RF voltages are required to achieve the same etch rates as conventional RIE systems. Due to higher etch rates, etching times are reduced. These two effects combine to result in reduced surface damage versus that observed in conventional RIE systems which is worse due to high energy collisions over long periods of time. The surface of the sample is not heated as much in ECR reactive ion etching, and in most ECR systems the sample is helium backside cooled to minimize the temperature increase. The net result is higher etch rates with less damage to the surface of the sample.

### 1.6 Theory of Reactive Ion Etching

As described previously, the two processes taking place during plasma etching are chemical reaction and ion bombardment sputtering. Chemical etching, independent of sputtering, has several distinctive characteristics. Reactive species, in the form of neutrals and radicals will attack the surface, breaking chemical bonds. The surface coverage of the reaction product will affect the rate at which this can take place. If the reactive species are small and can attack the surface independent of direction of impingement, the etching rate will be the highest. The products of these surface reactions will often be volatile and quickly leave the surface as gases composed of removed surface atoms. This is the etch

process. Figure 7 illustrates the type of etching that will be observed for chemical and sputter dominant processes respectively.

In the absence of sputtering, chemical etching will have a finite etch rate,  $R_c$ , for any given species.  $R_c$  is a function of many parameters. Since the reactions are diffusion controlled, the crystallographic orientation of the sample and extent of grain boundaries will be a factor. Typically wafers are grown off axis to create smooth surfaces and to avoid channeling of reactive species and increased chemical etching below the near surface. Activation energies are a concern since the stronger the bonding of the original sample, the more energy it will take to break the bonds and thus a larger flux of reactive species would be needed. For best results, the energy of formation of etch product bonding should be larger than the energy of formation of the original sample's bonds. Temperature will provide the energy to activate the reactions so,  $R_c$  will be a strong function of this parameter. Certainly  $R_c$  will be highly dependent on the rate of the chemical reactions and kinetics involved in the breaking of existing bonds and forming of new bonds. These kinetic steps can be diffusion limited, reaction limited, removal limited, etc. Finally, pressure in the chamber will affect  $R_c$ . As discussed above, increasing the pressure will increase the number of active species. Higher pressure will also reduce the mean free path of the sputtering ions thereby hindering surface bombardment. The result is an increase in  $R_c$ .

Sputtering, independent of chemical etching, has several distinctive characteristics. Ions created in the plasma will slowly drift toward the sheath region where they will be accelerated toward the sample with perpendicular trajectories. The impact of the ions with the sample will sputter atoms from the surface by inelastic energy transfers.

Repeated impacts remove multiple atomic layers through kinetic energy transfers. This is the sputter etch process. Sputtering leads to good control over feature shape since the trajectories are so uniform. The substance is preferentially etched at any surface exposed to the vertical bombardment. Non exposed regions are completely unetched. This results in near vertical sidewalls with good anisotropy as shown in Figure 7.

In the absence of chemical etching, sputtering will have a finite etch. This etch rate, designated as  $R_s$ , is a function of several parameters such as mass of the sample's constituents, energy of incident ions, etc. It is not, however, as complicated as the finite etch rate  $R_c$ .  $R_s$  is dependent heavily on the RF bias that is applied to the sample since this sets the maximum energy of the sputtering ions. As described previously, the magnitude

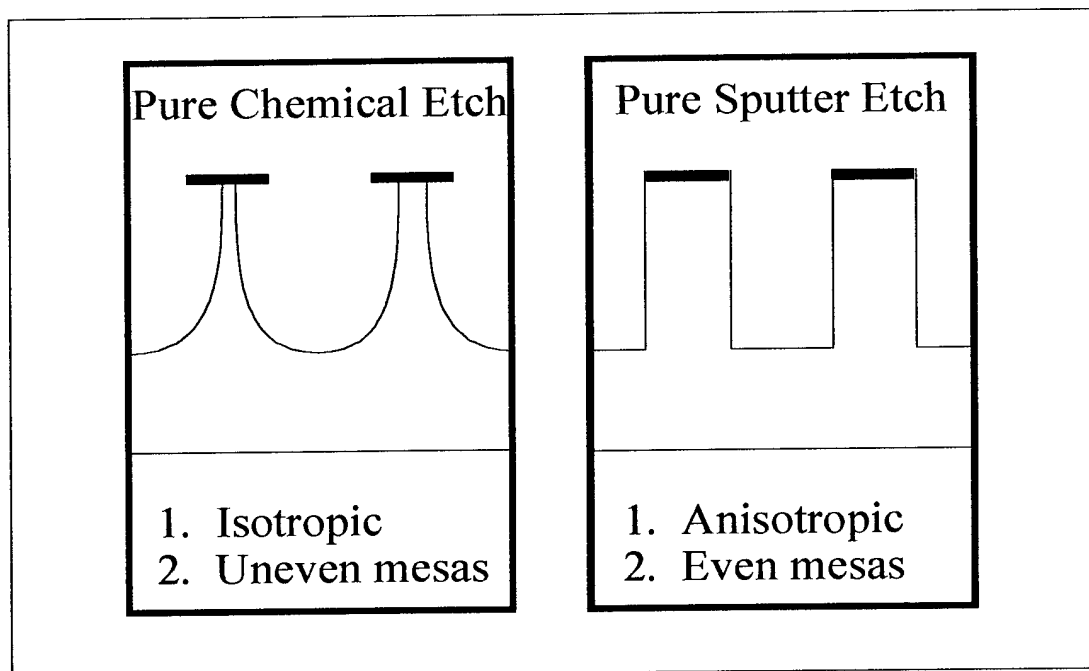


Figure 7. Comparison of pure chemical and pure sputter etching.

of the RF bias will determine the relative energy with which any given ion will reach the surface of the sample. Also previously mentioned was the affect of chamber pressure on

the mean free path of the sputtering ions. Higher pressures reduce  $R_s$  due to gas phase scattering. The molecular complexity of the ions will affect the sputter rate. Finally, individual ions will exhibit a mass dependence on the sputter rate. Ions with masses similar to atoms in the sample can conserve energy and momentum by transferring a maximum fraction of energy to the sample atoms. The energy transfer fraction for direct head on collisions depends on mass as:<sup>13</sup>

$$\frac{E}{E_0} = \left( \frac{m_1 - m_2}{m_1 + m_2} \right)^2$$

Equation 1. Mass dependence of the relationship between the scattered ion energy and incident ion energy when an elastic collision takes place.

For any grazing angle collision, the energy transfer will be reduced but by the cosine of the scattering angle. In all cases, regardless of mass, this will reduce the transfer by the same amount as long as the scattering angle is equivalent. When  $m_1 = m_2$ , all of the energy is transferred to the sputtered atom and the ratio becomes zero. If  $m_1 \ll m_2$  or  $m_1 \gg m_2$  the energy transferred is less and the fraction is increased. Maximum energy transfer will allow bond breaking and therefore sputtering. To a crude first approximation, the inverse of the ratio is a measure of the sputter yield due to the incident ions.

As discussed, the independent processes have finite etch rates. When the sputtering and chemical reactions are combined, a synergism takes place that results in an etch rate that is much greater than the sum of  $R_c$  and  $R_s$ .<sup>7</sup> This synergism, though widely documented, cannot be fully explained. However, it results from sputter-enhanced removal of volatile etch products and the regeneration of fresh surfaces. There is some

conflict of opinion as to whether the energetic broken bonds of sputtered surfaces are preferentially attacked by reactive species that volatilize quickly, or if the reverse is true. Volatile products are formed by reactions and then bombardment removes these species.

While the exact mechanism is unknown, there are three points,  $R_c$ ,  $R_s$ , and the synergism point that are readily known. Theory would suggest that if only one parameter is varied over an infinite range of values in the plasma, the etch rate should follow a continuous function that includes  $R_c$ , the synergism point, and  $R_s$ . Figure 8 is an example of this type of behavior. Clearly  $R_c$  and  $R_s$  are not required to be equal and the synergism point is not required to be in the middle of this curve. It is shown this way only for demonstrative purposes. In fact, for any given variable with a range over infinite values,

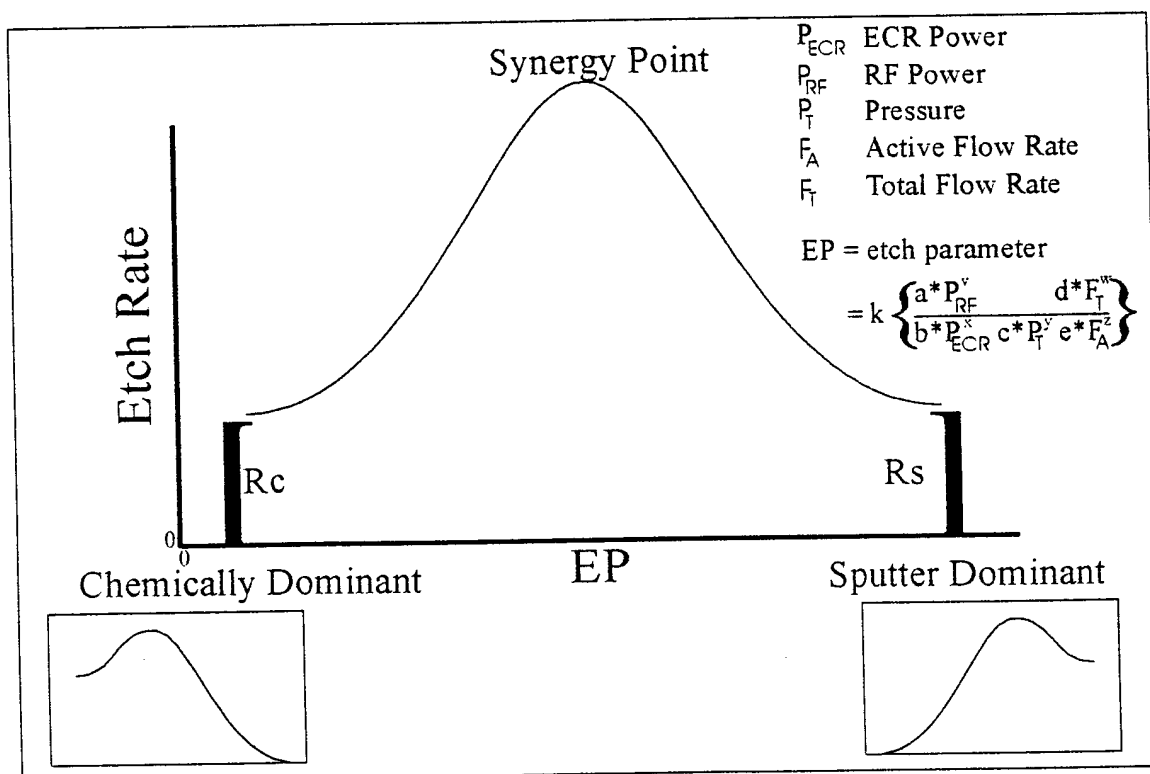


Figure 8. General example of the dependence of etch rate on a variable such as RF power, ECR power, pressure, or gas flow ratios over the full range of that variable.



there will be a uniquely distinctive curve of this type.

With this in mind, several general trends can be described. Increased ECR power will increase the ion and reactive radical densities within the plasma. The increase in reactive radical densities will clearly favor pure chemical etching. The increase in ion density should increase the rate of sputtering,  $R_s$ . This would be true if the accelerating potential remained constant. The plasma compensates for increased ion density by reducing the potential seen by the ions. This means that more ions will hit the surface but with reduced energies. Therefore, one can assume that increasing the ECR power from 0 to a substantially large power, the etch rate should vary as shown schematically in Figure.

Increasing RF power increases the energy of the ions bombarding the surface and has no effect on the active radicals and neutrals. One can therefore conclude that increasing the RF power from 0 to a substantially large power would result in a change in etch rate from near  $R_c$  toward  $R_s$  as indicated in Figure 8.

Varying the pressure in the chamber enhances chemical etching. Therefore one can conclude that increasing the pressure from 0 to substantially high pressures would result in a change in etch rate from near  $R_s$  toward  $R_c$  as indicated in Figure 8.

Finally, varying the ratio of the active gas flow rate with the carrier gas flow rate should increase the density of the reactive species and decrease the number of the ions for sputtering from the carrier species. Chemical dominance should result. Therefore, by varying the reactive constituent fraction from 0 to 1 the etch rate should change from  $R_s$  toward  $R_c$  as indicated in Figure 8.

In all cases there will be some synergy between the two mechanisms. It is impossible in the ECR or any RIE system to have pure chemical etching because even in

the absence of RF power a small bias is created between the sample and the plasma. Some sputtering, though low, will occur. It is also likewise impossible to have a purely sputter mechanism unless nonreactive gases are used such as pure Ar etc. Using reactive gases requires some chemical etching though it may be minimized.

## CHAPTER 2 EXPERIMENTAL PROCEDURES

### 2.1 Samples

Wafers of 0.33mm thick 6H-SiC were purchased from Cree Research Incorporated. The wafers were grown  $3.5^\circ \pm 0.5^\circ$  off {0001} axis toward  $\langle 1120 \rangle \pm 10^\circ$  on Si substrates and polished on the silicon terminated face using patented techniques by Cree Research. This growth technique was used to obtain uniform smooth layered films. It also helps reduce the probability of channeling during the patterning processes. The wafer used for roughness and surface analysis in this experiment was n-type with a doping concentration of  $2.8 \times 10^{17}$  nitrogen atoms/cm<sup>3</sup>. The wafer was sectioned with a diamond scribe into  $\sim 3\text{mm}^2$  pieces for analysis. No additional sample preparation was performed on this material. Samples  $\sim 3\text{-}4\text{mm}^2$  of 3C-SiC grown on Si were supplied by Lucent Technologies Bell Laboratories for the purposes of etch rate determination. A carbon paste pen was used to apply a dot to the surface of each of these samples for masking for determination of the etch rate.

ECR plasma etching was performed in a Plasma-Therm IP Model SLR 770 system (see Figure 3). The system had two chambers. One was the sample load lock and the other was the plasma chamber which remained at vacuum of approximately  $1 \times 10^{-6}$  Torr during sample exchange. The plasma chamber was flushed with pure nitrogen for approximately 20 minutes before etching in order to reduce oxygen and water vapor

contamination that normally adheres to chamber surfaces. SiC samples were glued to a silicon wafer with vacuum grease and loaded into the load lock chamber at atmospheric pressure. The load lock chamber was reduced to a vacuum equivalent to the plasma chamber and the silicon wafer transferred by mechanical arm to the plasma chamber stage. The sample stage holding the Si wafer in the plasma chamber was a helium backside cooled electrode biased with 13.56 MHz RF. It was not exact, but to a first approximation, the numerical value of the RF wattage was equal to the numerical value of the negative voltage between the plasma and the sample electrode in V. The plasma was created in the Plasma Therm by supplying 170 A to the upper magnet and 40 A to the lower magnet. A 2.45 GHz ECR voltage was applied to create the plasma. In all experiments, the total flow rate in standard cubic centimeters was constant. The ratio of flow rates between the reactive and carrier species was varied from 0 to 1. Each sample was etched for 1 min. under these conditions.

The samples were removed from the reactor and the carbon paste masks on the 3C-SiC samples were removed with acetone and tetracycloethylene. This additional treatment was not performed on the 6H-SiC samples. Dektak stylus profilometry was used to determine etch rates.<sup>11</sup> Surface morphology of the 6H-SiC samples was measured using atomic force microscopy (AFM).<sup>11</sup> Auger electron spectroscopy (AES) was used to determine the composition of the surface for detection of contamination with etch gases and the type of termination of the SiC lattice.<sup>11</sup>

## 2.2 Etching Conditions

Gas mixtures used for etching contained argon or hydrogen as carriers and chlorine, iodine bromide, or sulfurhexafluoride as chemically active gases. Argon plasmas without active gas species were used to test pure sputter etching. All experiments used a total flow rate of 15 sccm except experiments involving IBr where 8 sccm was used. Ten experiments were performed with each argon/active gas mixture and four were performed with  $\text{Cl}_2/\text{H}_2$ . The conditions for each experiment are shown below in Table 2. For each

Table 2. Range of experimental conditions studied using 3C-SiC. (\* - indicates where 6H-SiC was used in addition to 3C-SiC for analysis of surface morphology and surface composition).

Plasma (Standard)	ECR (Watts) (1000)	RF (Watts) (150)	Pressure (mT) (1.5)	Active Fraction (.667)
$\text{Cl}_2/\text{H}_2$	400-1000*	150	1.5	.667
$\text{Cl}_2/\text{Ar}$	400-1000	50-250	1.5	0 -1
$\text{SF}_6/\text{Ar}$	400-1000	50-250*	1.5-10	.667
IBr/Ar	400-1000	50-250	1.5	0-1*
Ar	400-1000	50-350*	1.5-10	1

range tabulated, a series of experiments was run that range with the remaining variables held constant at the designated values in the (Standard) row. For example, with the chlorine experiments, the following experiments were performed.

- 1) ECR Microwave power was varied from 400-1000 Watts in 10  $\text{Cl}_2/5$  Ar at a process pressure of 1.5 milliTorrr and 150 Watts of RF power.

- 2) Experiments identical to 1) were run with the  $\text{Cl}_2/\text{H}_2$  environment.
- 3) RF bias effects were studied using 10  $\text{Cl}_2/5$  Ar, 1000 Watts of microwave power, 1.5 milliTorr, and 50-250 Watts of RF power.
- 4) Finally, chemical effects were studied by maintaining 1000 Watts ECR power, 1.5 milliTorr, 150 Watts RF power and varying the flow rate of the chlorine and the argon such that the ratio of the chlorine flow rate to total flow rate varied from 0-1. This ranged from 15 sccm pure argon to 15 sccm of pure chlorine.

3C-SiC was used for every experiment performed for etch rate analysis. The \* indicates the experimental conditions for which 6H-SiC was also used for analysis of roughness and composition of the terminated surface.

### 2.3 Characterization

#### 2.3.1 Stylus Profilometry

Each etch was performed for 1 minute. This allowed for simple determination of the etch rate in Å/minute using stylus profilometry on a Veeco Instruments Inc. Dektak IIA.<sup>11</sup> The technique for measuring the depth of etching was fairly simple and is illustrated in Figure 9. The stylus was 90° diamond tip with a radius of ~ 10 nm that was lowered to the surface of the sample. It then was dragged in one direction toward the sidewall created during the etching process. The surface profile in one direction was traced by deflections up or down according to surface features. The needle movement was interfaced with a computer which amplified the signal due to changes in vertical height of the tip. The sidewall thus appeared as a large deflection from the zeropoint up

to the height of the unetched section. A typical trace is shown in figure 9 for a deflection of 560 Å.

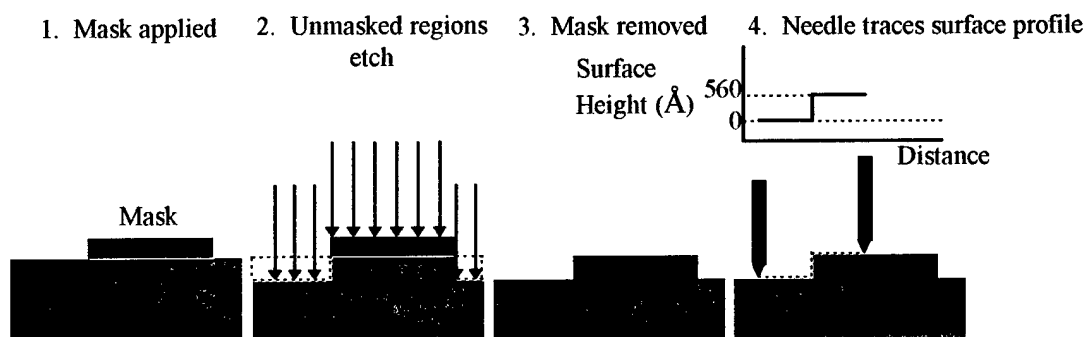


Figure 9. Schematic of the procedure used to determine etch rate.

### 2.3.2 Atomic Force Microscopy (AFM)

AFM was performed on the 6H-SiC unmasked samples using a Digital Instruments Nanoscope III Multimode Scanning Probe Microscope to determine the change in roughness associated with the plasma etching.<sup>11</sup> AFM is very similar to stylus profilometry however it is much more sensitive to small changes ( $\sim 1$  Å) in surface height. A fine reflective silicon cantilever (coated with native silicon dioxide) with a radius of  $\sim 10$  nm was used as the tip which traveled across the surface. A laser was aligned with this tip. The laser amplified small vibrations of the tip because the detector for the reflected signal was several inches away from the cantilever. The assembly with the tip was then lowered toward the surface to within a few Å. In the tapping mode of AFM, the tip was vibrated relative to the surface at frequencies of 320-350 Hz with drive amplitudes of 120 - 450 mV. The amplitude of this deflection was a measure of the height of features on the surface. The diagram in figure 10 shows this process.

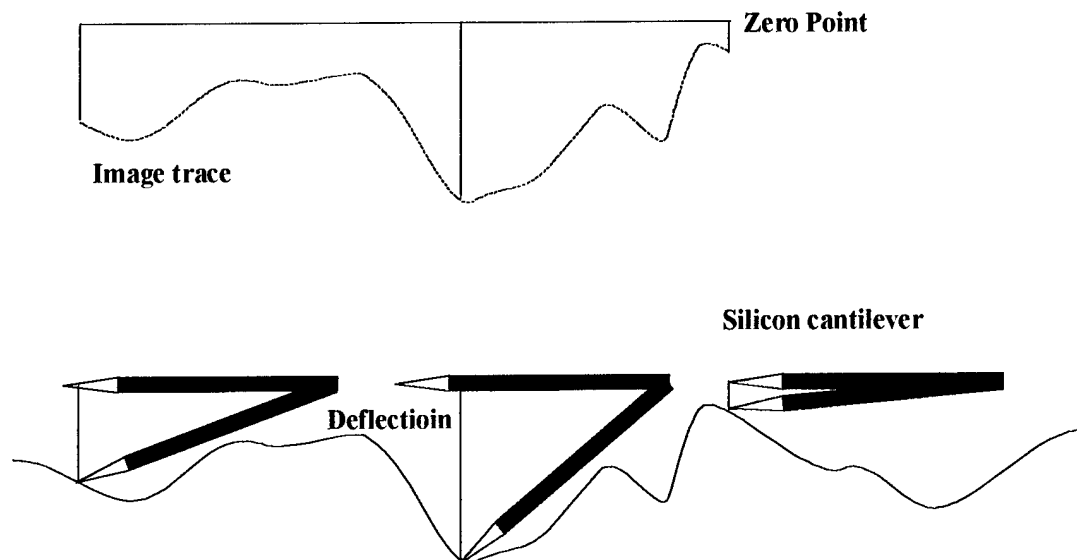


Figure 10. AFM cantilever motion and the resulting information for a single trace in the x-direction. Multiple scans along the x-axis are made as the tip moves along the y-axis to result in a two dimensional image of the surface topography.

### 2.3.3 Auger Electron Spectroscopy (AES)

AES was performed using a Perkin Elmer Phi 660 Scanning Auger Multiprobe as a chemical analysis technique for the SiC surfaces.<sup>11</sup> This technique used the unique energy level scheme for electrons in an element as a measure of the concentration of given elements on the surface of the SiC samples. When an atom was bombarded by a beam of energetic primary electrons, ionization may lead to either photon or Auger electron emission as shown in Figure 11. In the case of valence band ionization, an electron from the outer shell of the chlorine atom was removed. The remaining chlorine ion was in the ground state and was stable. In the second situation, an energetic electron removed a core level electron from the 2p and 2p levels. In the final case, the energy was not given off as a photon but was used to stimulate the removal a third electron. This electron is known



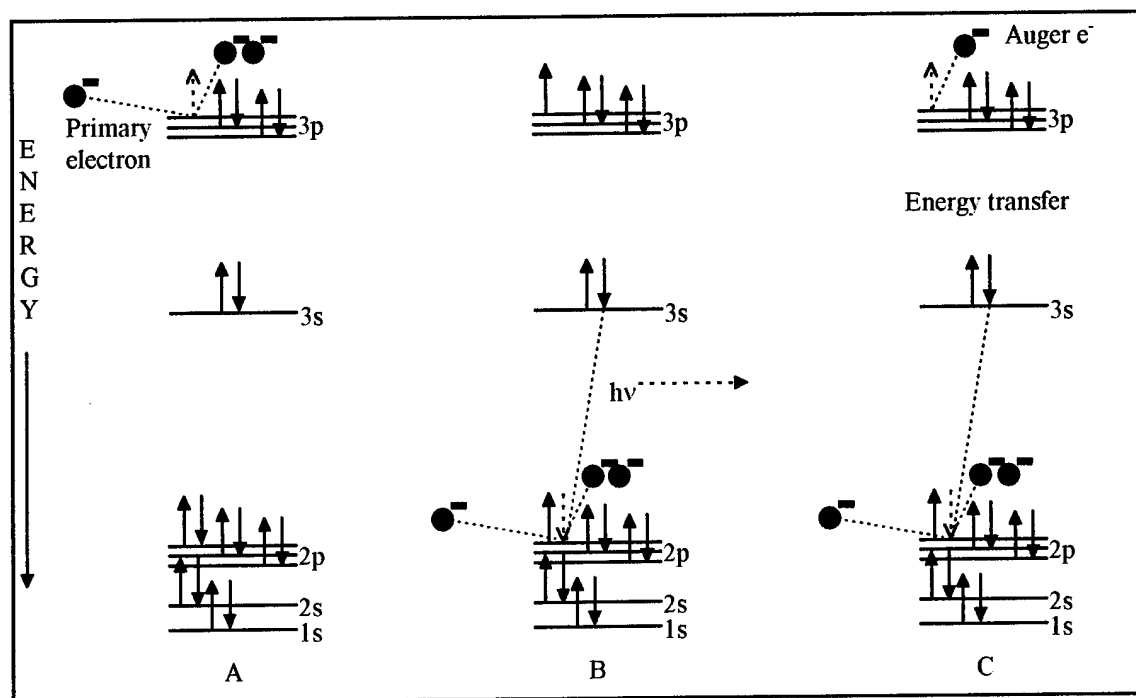


Figure 11. Electron energy level representations of A) valence band ionization, B) core level ionization and photon emission, and C) core level ionization and Auger emission as a result of electron impact on chlorine.

as an Auger electron and it has a kinetic energy related to the energy given off by the lower level transition ( $E_{2p} - E_{3s}$ ) minus the binding energy of the level from which it was emitted ( $E_{3p}$ ). Thus the energy of this electron is a fingerprint of the chlorine. Since the Auger electrons only escape from about the first 10 Å of the surface, a detector which analyzes the energies and intensities of Auger will determine the chemical composition of the surface of a sample. By in situ sputtering, AES can be used to determine the composition versus depth of the sample to determine the extent to which contaminants accumulate on the sample either through diffusion, implantation, or channeling along crystallographic planes.

## CHAPTER 3 RESULTS AND DISCUSSION

### 3.1 Etch Rate 3.1.1 Etch Rate Results

The etch rate data are arranged and tabulated with respect to the variable being investigated. Comparisons will be given between the different plasma chemistries.

In the experiments during which ECR power was varied between 400 and 1000 Watts, pressure was maintained at 1.5 milliTor, RF power was held at 150 Watts, the ratio of the flow rate of the active species to the total flow rate was held constant at 0.667 and the etch time was one minute. The results in Table 3 and Figure 12 show that sulfur hexafluoride had the highest etch rate up to 600 Watts.  $\text{Cl}_2/\text{Ar}$  had higher etch rates above

Table 3. Etch rate in Å/min as a function of ECR Power for a total pressure of 1.5 mTorr, 150 Watts RF power, and constant flow rate ratio. (\* indicates the ratio of active to total flow rates for that gas chemistry).

ECR Power (W)	Ar (1)*	$\text{Cl}_2/\text{Ar}$ (.667)*	$\text{Cl}_2/\text{H}_2$ (.667)*	$\text{SF}_6/\text{Ar}$ (.667)*	$\text{IBr}/\text{Ar}$ (.5)*
400	600	900	1100	2000	1000
600	600	1700	1200	1900	1200
800	600	2100	1100	1600	600
1000	800	2600	700	1300	900

this power. Argon had the lowest etch rate, while  $\text{SF}_6$  exhibited a near linear decrease from 2000 to 1300 Å/min. With increasing power,  $\text{Cl}_2/\text{Ar}$  showed a near linear increase from 800 to 2600 Å/min.  $\text{Cl}_2/\text{H}_2$  exhibited a small negative curvature etch rate curve with a maximum at 1200 Å/min. It decreased to 1800 Å/min at low ECR power and 800

$\text{\AA}/\text{min}$  at higher microwave powers. IBr/Ar data were sporadic. It averaged approximately 1000 to 800. The 800 Watt experiment yielded values for etch rate as low

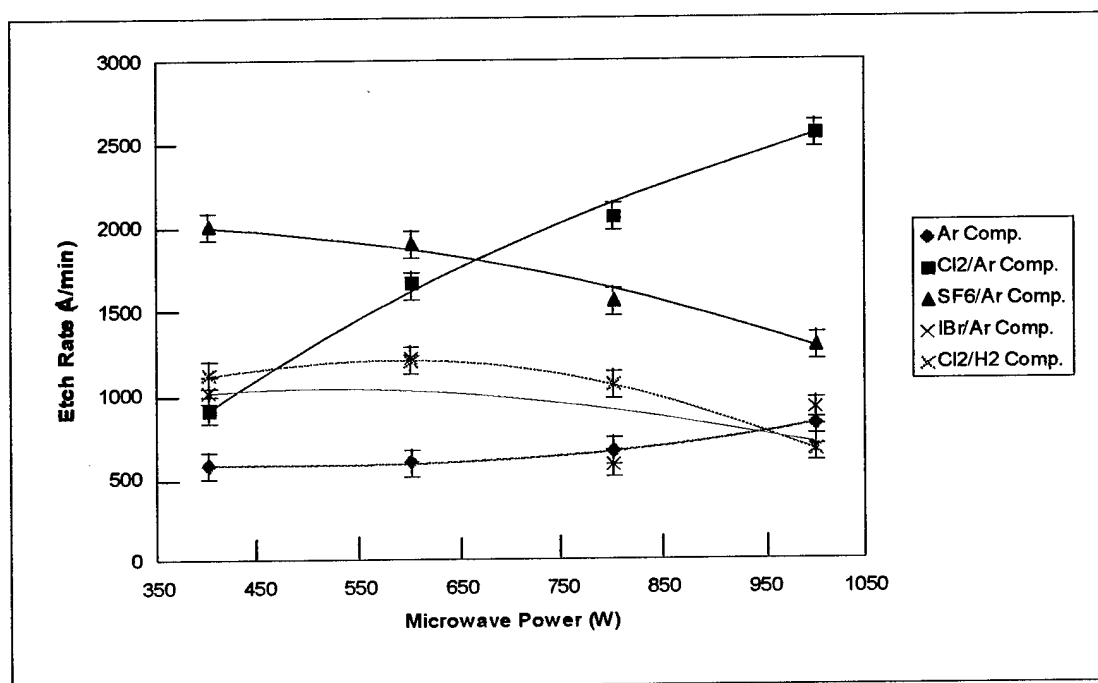


Figure 12. Etch rate in  $\text{\AA}/\text{min}$  as a function of ECR Power for a total pressure of 1.5 mTorr, 150 Watts RF power, and constant flow rate ratio.

as 450  $\text{\AA}/\text{min}$  and as high as 730  $\text{\AA}/\text{min}$ . The average of these values is reported in the tables, but obviously the error bars are quite large, therefore, the shape of the curve is inconclusive. Argon showed a nearly linear increase from 550 to 800  $\text{\AA}/\text{min}$  with increasing power.

In the experiments in which RF power was varied, pressure was maintained at 1.5 milliTorr, ECR power was held at 1000 Watts, the ratio of the flow rate of the active species to the total flow rate was held constant. The results shown in Table 4 and Figure 13 show that sulfur hexafluoride/argon had the highest etch rate ( $\sim 2500 \text{ \AA}/\text{min}$ ) of all plasmas studied. The data for SF<sub>6</sub>/Ar 150 Watts RF is considered to be spurious since it is

very low, but, there are no reasons to believe that the etch rate would exhibit a minimum in RF power at 250 W. For the best fit curve, it is ignored.  $\text{Cl}_2/\text{Ar}$  closely rivaled the

Table 4. Etch rate in  $\text{\AA}/\text{min}$  as a function of RF power for a total pressure of 1.5 mTorr, 1000 Watts ECR power, and constant flow rate ratio. (\* indicates the ratio of active to total flow rates for that gas chemistry).

RF Power	Ar (1)*	$\text{Cl}_2/\text{Ar}$ (.667)*	$\text{SF}_6/\text{Ar}$ (.667)*	$\text{IBr}/\text{Ar}$ (.5)*
50	Not Tested	0	2100	200
100	(Lost)	1300	2500	900
150	800	2600	1300	900
250	500	900	2700	1100
350	900	Not Tested	Not Tested	Not Tested

etch rate of  $\text{SF}_6/\text{Ar}$  only at 150 Watts RF. On average, Argon had the lowest etch rates ( $\sim 800 \text{ \AA}/\text{min}$ ) of all the chemistries.

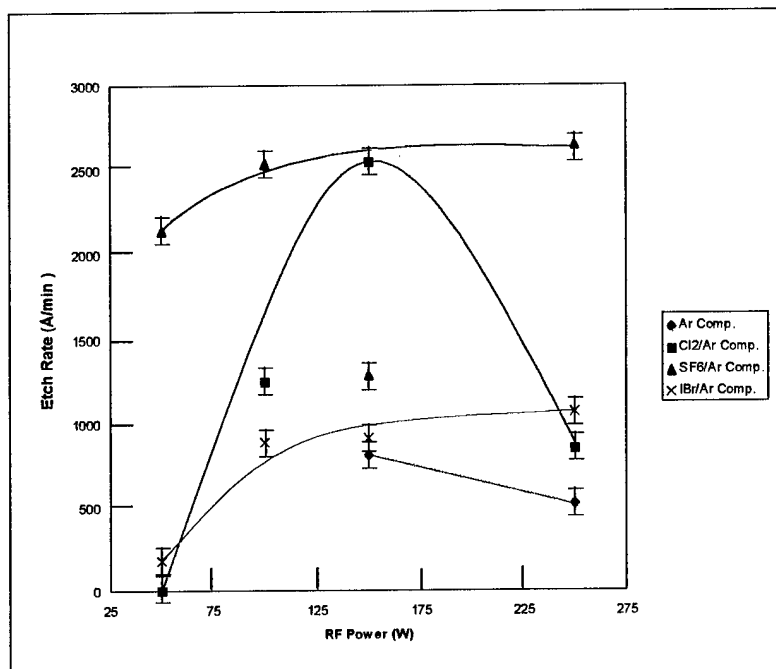


Figure 13. Etch rate in  $\text{\AA}/\text{min}$  as a function of RF power for a total pressure of 1.5 mTorr, 1000 Watts ECR power, and constant flow rate ratio.

In the experiments in which pressure was varied, ECR power was held at 1000 Watts, RF power was held at 150 Watts, the ratio of the flow rate of the active species to

the total flow rate was held constant and the etch time was one minute. The results are shown in Table 5 and Figure 14. Sulfur hexafluoride had the highest etch rate of the two

Table 5. Etch rate in Å/min as a function of plasma chamber pressure for 150 Watts RF power, 1000 Watts ECR power, and constant flow rate ratio. (\* indicates the ratio of active to total flow rates for that gas chemistry).

Pressure (mTorr)	Rate (Å/min) Ar (1)*	Rate (Å/min) SF <sub>6</sub> /Ar (.667)*
1.5	800	1300
5	500	3400
7.5	700	3600
10	800	3900

gas chemistries studied and it exhibited a monotonic increase from 1300 to 4000 Å/min as pressure was increased from 1.5 to 10 milliTorr. Argon shows a nearly constant etch rate with an average of ~700 Å/min.

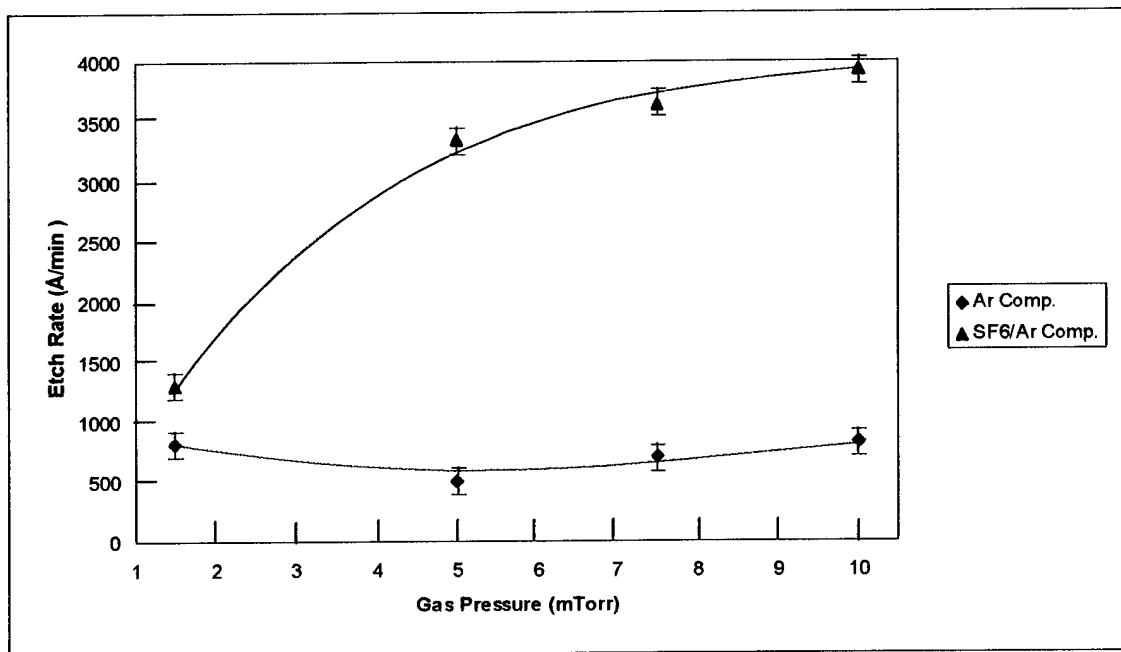


Figure 14. Etch rate in Å/min as a function of plasma chamber pressure for 150 Watts RF power, 1000 Watts ECR power, and constant flow rate ratio.

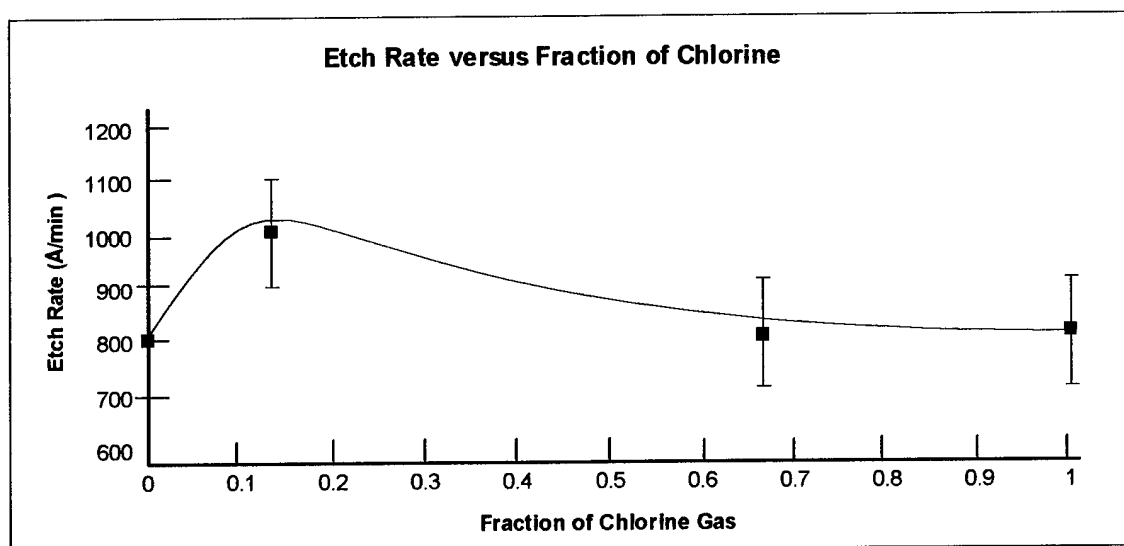
In the experiments in which the ratio of the flow rate of the active species to the total flow rate was varied, ECR power was held at 1000 Watts, RF power was held at 150

Watts, the pressure was held at 1.5 milliTorr and the etch time was one minute. The results in Table 6 and Figure 15 show that  $\text{Cl}_2/\text{Ar}$  had the highest etch rate and the widest

Table 6. Etch rate in  $\text{\AA}/\text{min}$  as a function of active to total flow rate ratios for 150 Watts RF power, 1000 Watts ECR power, and for a total pressure of 1.5 mTorr.

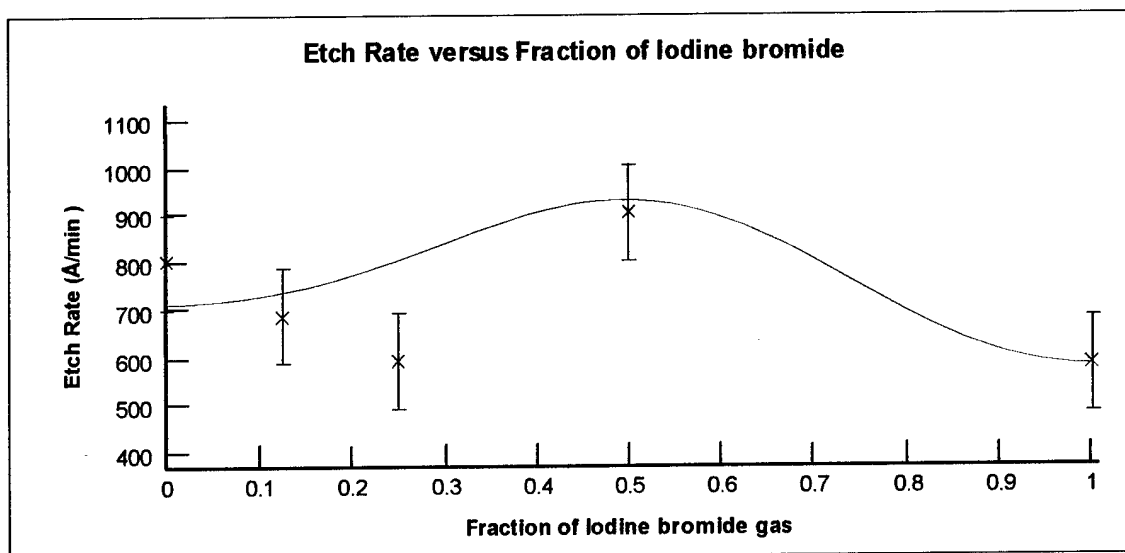
$\text{Cl}_2$ flow rate divided by total flow rate	Etch Rate ( $\text{\AA}/\text{min}$ )		IBr flow rate divided by total flow rate	Etch Rate Rate ( $\text{\AA}/\text{min}$ )
0	800		0	800
0.133	1000		0.125	700
0.667	800		0.25	600
1	800		0.5	900
			1	600

variation of the two gas chemistries studied. The etch rate was skewed right with a maximum at 1000  $\text{\AA}/\text{min}$ . Iodine bromide also showed an etch rate curve with a maximum around 900  $\text{\AA}/\text{min}$ .



a)  $\text{Cl}_2/\text{Ar}$

Figure 15a. Etch rate in  $\text{\AA}/\text{min}$  as a function of active to total flow rate ratios for 150 Watts RF power, 1000 Watts ECR power, and for a total pressure of 1.5 mTorr for  $\text{Cl}_2/\text{Ar}$ .



b) IBr/Ar

Figure 15b. Etch rate in Å/min as a function of active to total flow rate ratios for 150 Watts RF power, 1000 Watts ECR power, and for a total pressure of 1.5 mTorr for IBr/Ar.

### 3.1.2 Etch Rate Discussion

#### 3.1.2.1 Dependence on ECR Power

The effect of ECR Power was studied for all chemistries. Argon had the lowest etch rate of all the plasma gas chemistries, as expected, because there is no chemical etching taking place. Argon is a pure sputter etchant and on the etch rate curve described in figure 8, argon is completely to the right where  $R_s$  is the observed etch rate. It is expected to be lower than all the other gases because there are no synergistic effects between sputtering and gaseous reactions.

IBr/Ar resulted in an etch rate that was only slightly higher than argon. This is somewhat surprising since iodine and bromine are noted for their high reactivity. Iodine and bromine ions are also very massive which intuitively might be expected to cause high sputter yields. However as shown by Equation 1, this expectation is false. Silicon has an atomic mass of 28.9 AMU while carbon has a mass of only 12.01 AMU. As previously

discussed in chapter 1, in order for conservation of energy and momentum during collisions leading to sputtering, the maximum energy transfer takes place between atoms whose masses are similar to the sputtering ion. Table 7 shows the inverse of the ratio of the energy of the ions after collision to their incident energy for all gases in this study. This is reported as  $E_o/E$ . To a rough approximation, this ratio is an indicator of the sputter yield for these gases. Ar has a mass of 39.95 AMU so it's incident to scattered

Table 7. Estimation of sputter yield using the mass comparison relationship between the incident ions and the sputtered species, carbon and silicon.

Gas	Mass (AMU)	$E_o/E$ for Carbon	$E_o/E$ for Silicon
Argon	39.95	3.45	38.82
Bromine	79.9	1.83	4.55
Chlorine	35.45	4.09	96.51
Fluorine	19.0	19.68	23.40
Hydrogen	1.0	1.39	1.14
Iodine	126.9	1.46	2.52
Sulfur	32.0	4.84	385.93

energy is 38.82 for Si and 3.45 for C which will lead to high sputter rates. Iodine has a mass of 126.9 AMU so any collisions with these particles will result in very little energy transferred and will not contribute much to sputter enhanced removal of etch products. Br ions (79.9 AMU) though much less massive are still two and a half times more massive than silicon and are almost seven times more massive than carbon. These ions will also transfer little energy to the sample, thus, there is no advantage of sputtering with I and Br ions which is shown with the low etch rates in Figure 12 and Table 3. Chemical reactions will take place as the neutral I and/or Br atoms reach the surface, but clean surfaces cannot be created quickly since only half of the ions contained in the plasma cause



collisions. The I and Br ions will lower the sputter rate of the surface. Ar ions simply cannot keep up with the reaction rate to give a good synergism.

Chlorine based chemistries show large differences in etch rates between  $H_2$  and Ar carriers. In general, these differences in etch rate are much greater than in iodine bromide chemistries. For Ar carrier gas chemistries, the etch rate quickly increased as ECR power increased. This trend was expected since chlorine ions have a mass of 35.45 AMU. At low ECR powers, it is possible to ionize the  $Cl_2$  molecule without dissociating it. This would have a mass of 71 AMU and would tend to be more elastic in its collisions. Also, because of dissociation of the molecular ion at the surface upon impact, the energy of the resultant atomic species is lower and sputter would be decreased as shown in Figure. As the ECR power increased, more ions would be produced and molecular dissociation would increase to create higher energy ions that were better matches in mass. In addition to the combined sputtering by Ar and chlorine ions, chlorine would quickly react with the surface. Thus synergy was high between the sputtering and chemical reactions.

For  $H_2$  carrier with chlorine, the rate was substantially reduced. The etch rate had a peak at 1200 Å/min and then decreased slowly. This can be explained with several arguments. First of all, H ions have a mass of only 1 AMU. They can not sputter the surface at a rate as high as argon does because mismatched masses. Few sputtering collisions could take place. The plasma as a result lost many of its sputtering ions. Secondly, hydrogen is a reactive gas and it may have passivated the surface of the silicon carbide by formation of energetically favorable surface layers. Sputtering could not easily remove this passivant and allow chlorine chemical reactions to take place. The result would be a lowering of the etch rate because only the sputtering mechanism of the

chlorine was able to take place. The maximum etch rate therefore corresponds to the maximum rate of sputtering and reactivity of the chlorine alone. In Figure 12, to the right of the maximum at high ECR powers where normally chemical dominance would take place, the hydrogen was masking the surface too much for the chlorine to react. To the left of the maximum at low ECR powers, the sputtering mechanism was dominating and chlorine wasn't able to react synergistically.

In addition to passivation effects, the etch rates were lowered compared to etch rates with argon carrier gas plasmas because of mass matching. Table 7 shows that the estimated sputter yield for argon is three times higher than hydrogen for carbon and almost forty times more effective for sputtering silicon. Thus, even if passivation effects are minor, there should still be a notable decrease in etch rates which was seen in Figure 12.

Finally in the  $\text{SF}_6$  case, higher etch rates were seen at lower ECR power because the reactivity of the fluorine was synergistically favored by the sputtering. Fluorine had a mass of 19 AMU so it sputtered carbon and silicon very efficiently. Sulfur has a mass of 32 AMU so all species in the plasma that are ionized helped with sputtering. The high reactivity of fluorine created maximum synergy when sputter rate was high. As the sputter rate was reduced at high ECR powers, the rate was drastically reduced, because much like hydrogen, fluorine reacted quickly to cover the surface of the SiC. If sputter enhanced removal was reduced, reaction rate was diffusion dominant and the etch rate was reduced because of passivated surfaces.

### 3.1.2.2 Dependence on RF Power

The effect of RF Power was studied for all chemistries except chlorine with hydrogen as the carrier gas. The etch rate would ideally vary directly with the energy of the particles hitting the surface in eV if there was nothing to compete with the sputter process. Thus  $R = C \cdot V$  where  $C$  is simply the constant of proportionality,  $R$  is the etch rate, and  $V$  is the voltage accelerating the positive ions from the plasma to the sample. The relation between power and etch rate is as follows.<sup>14</sup>

$$\begin{aligned} \text{Rate} &= C \cdot V & \sqrt{\text{Power}} &= C \cdot V \\ \text{Power} &= \frac{V^2}{R} & \text{Rate} &\propto \sqrt{\text{Power}} \\ \sqrt{\text{Power}} &= \frac{V}{\sqrt{R}} \end{aligned}$$

Calculation 1. A calculation relating the dependence of etch rate on bias power.

Therefore etch rate should vary with the square root of power. The fact that the etch rate curves do not exactly overlap the theoretical model indicates that they were described by complex functions that were a result of factors not limited to pure sputtering. However, since sputtering was taking place, the etch rate curve should rise quickly and then asymptotically approach a fixed value. The etch rate for  $\text{SF}_6$  exhibited a saturation over a range of 2100 to 2600 Å/min. IBr/Ar data increased from 100 Å/min until it showed an asymptotic saturation at 1000 Å/min. One would expect saturation with argon since it was purely sputtering. As shown in Figure 13, saturation around 800 Å/min did occur for the higher RF powers. Unfortunately, lower RF power analysis was unavailable. The

sample for 100 Watts RF power was lost in the analysis process, therefore, the data is missing. To prove that the etch rate curves in Figure 13 are not purely sputtering, simulations have been created to show the basic functions that would be necessary to give the observed starting and finishing points for each graph. These simulations, shown in Figure 16, were designed by following the simple procedure described above in the relationship between etch rate and voltage. In order to have each theoretical curve begin where the experimental curves begin, constants were added to each equation. The multiplication factors were chosen only to cause saturation of each curve at the same value as shown in the experimental curves. Clearly, without these additions, it would be impossible to even closely fit the data. It can be assumed that these correction factors from the pure sputtering models are approximating the effect of chemical etching in the synergism. Figure 16 shows the theoretical etch rate curves.

Iodine bromide had the next highest etch rate for varying RF powers. This was expected since as described above, the mass mismatch results in I and Br ions contributing very little to the sputtering process. The etch rate curve in Figure 13 deviates drastically from the theoretical curve shown in Figure 16 at low RF powers. This is consistent with etching theory because the chemical etching of the sample is dominant. Synergism improved as the RF power was slightly increased. After too large an increase, the reduced rate may be explained by slower chemical reactions rate limited by large surface coverage. Sputtering began to dominate more and the curve aligned more with the theoretical pure sputter curve at higher RF powers for IBr/Ar.

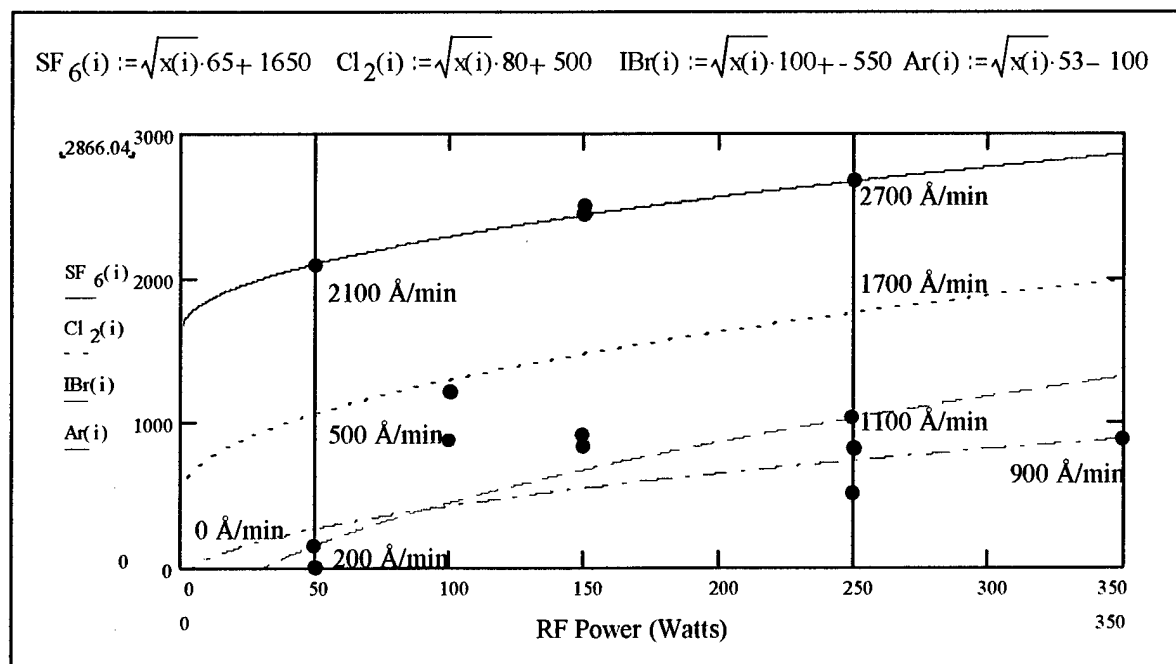


Figure 16. Calculated theoretical etch rates as a function of RF power compared to measured etch rates.

Sulfur hexafluoride had the highest etch rate for variable RF powers for reasons described previously. In this case, as with IBr, chemical etching could dominate at low RF biases. As RF power was increased, synergy between chemical reaction and sputter etching was reached at near 100 W. Above approximately 100 Watts, etching became more sputter dominant since chemical reactions became rate limited by surface coverage of fluorine. Interestingly, this saturation occurred at a higher RF power (approximately 150 Watts) than with the iodine bromide (100 Watts). This suggests that fluorine reactions are faster than iodine bromide and fluorine in general is more reactive than the other two species. Thus surface coverage was not rate limiting until higher RF biases.

Finally, Cl<sub>2</sub>/Ar showed a nearly parabolic curve in Figure 13 which mimicked the theoretical etch rate curve shown in Figure 8. In this case, we see all regions of the theoretical etch curve. For other chemistries, there were no clear maxima. It is clear however that at higher RF powers all gas chemistries fit the theoretical curves much more

closely than at low RF powers. This suggests that each gas chemistry did go from some level of chemical dominance to almost pure sputter etching as the RF power increased. One can only conclude that for some reason, chlorine chemistries had a higher synergy at the maximum etch rate than did the other plasma chemistries. The reason for this is not known.

### 3.1.2.3 Dependence on Total Pressure

The effect of total pressure was studied for Ar and SF<sub>6</sub>/Ar. Argon had a lower etch than SF<sub>6</sub>/Ar. When the pressure of the chamber was increased and the power held constant, the ion flux should have been nearly constant. However, at higher pressures, the mean free path for the ions would be reduced for sputtering. Sputtering rates should be hindered. For pure argon plasmas, where there were no chemical reactions, the reduction in sputtering should correlate to a reduction in etch rate. Argon ions were increased in number due to higher pressures, however, sputtering that would be enhanced by this increase in ion density is canceled by the reduction in mean free path. The net effect should be either a small reduction in etch rate or no change at all. This was generally what was seen in Figure 14.

Sulfur hexafluoride showed a factor of three increase in etch rate as the pressure was increased. The large sulfur hexafluoride molecules had a much greater effect on the reduction of the mean free path of the sputter species. Thus what was seen at low pressures was a dominant sputter mechanism near R<sub>s</sub> on the theoretical etch rate curve. As the pressure was increased, the synergism point was approached as sputtering was

complimented with more chemical reactions because the density of the active species was increased. This was seen as a leveling off of the etch rate.

#### 3.1.2.4 Dependence on Flow Rate

The effect of fractional flow rate of the active species was studied for IBr/Ar and Cl<sub>2</sub>/Ar. In both cases, the range of the ratio of active to total flow rates was 0 to 1. Characteristic etch rate curves were expected which mimic a variation of the theoretical curve in Figure 8. This was observed as shown in Figures 15 a) and b) especially for the chlorine data. The chlorine data distribution demonstrates the point made earlier in the theory section that the synergy point will not always be centered on the x-variable axis. In this case it is far to the left of that point.  $R_c$ ,  $R_s$  and the synergy point are clearly visible.  $R_c$  just happens to be almost exactly equal to  $R_s$ . Again recall that though  $R_s$  is truly defined,  $R_c$  is not exact because some sputtering with chlorine ions will occur even in a system purely composed of chlorine gas at 0 volts RF bias. Even with no applied bias, the self bias created by the sample stage to create an equilibrium of ion and electron fluxes for charge neutrality of the plasma, will accelerate positive chlorine ions to the surface with small energies. This will cause some sputtering contribution. Therefore, it is impossible to get an exact value of a pure chemical etch rate.

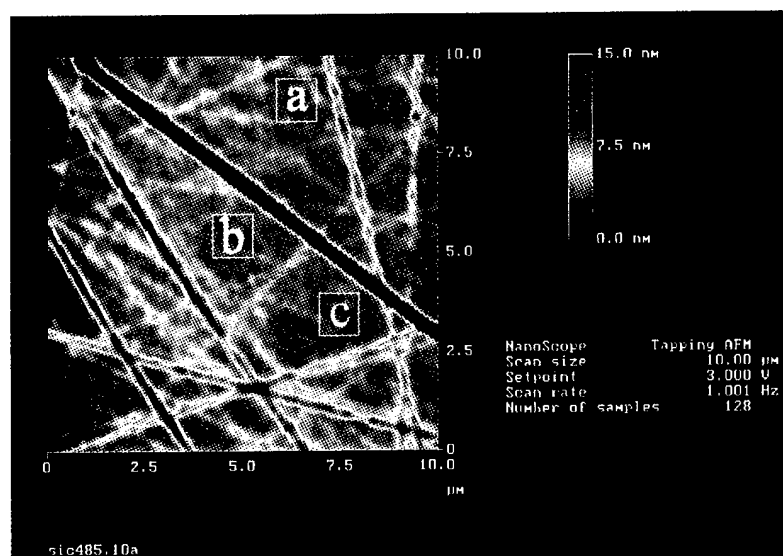
In the IBr case, the data require a little more explanation. The measured average etch rate for pure argon is 800 Å/min which is higher than with iodine bromide additive plasmas. Note that the argon curve is constant around 600-700 Å/min for all ECR powers except 1000 Watts. The 1000 W data point may be falsely high since the error in the Dektak stylus Profilometry surface step is estimated to be +/- 50-100 Å. This value is

obtained from the average variability noted in different measurements of etch rate for each individual sample. In any case, with error taken into account the curve shown in Figure 16 is believable and is expected. In this case, the synergy point is at .5 much further right than in the chlorine case. In this case  $R_c$  and  $R_s$  are not equal.  $R_c$  is roughly 600 Å/min while  $R_s$  is roughly 800 Å/min.

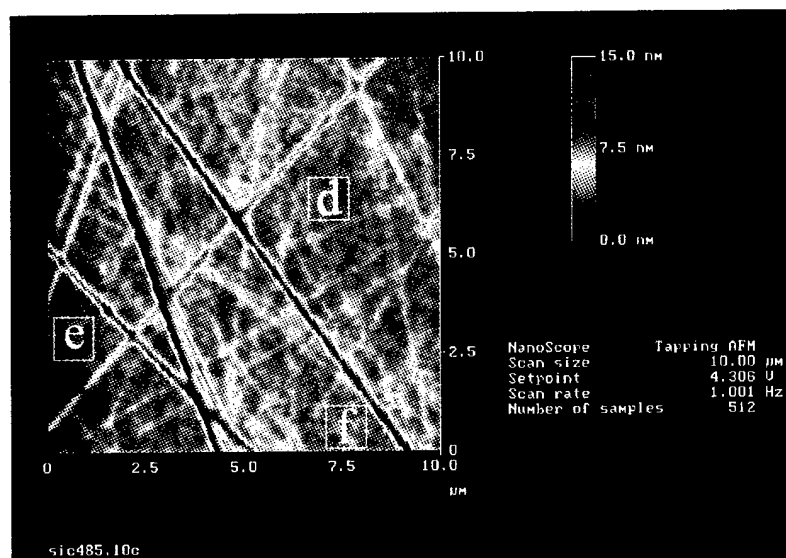
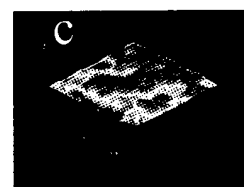
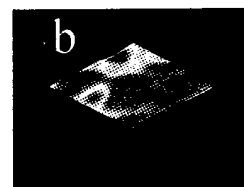
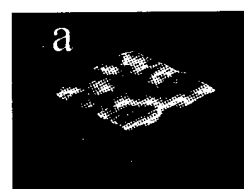
### 3.2 AFM

AFM was used to determine the surface roughness for each of the 6H SiC samples. Two 10 x 10 µm images were taken for each sample etched. RMS roughness was calculated from six to eight 1 x 1 µm sections for each of these images and the data was averaged for each sample. This was necessary since, as shown in Figure 17, there were an abundance of scratches that were artifacts of the polishing process employed by the supplier, Cree Research. These scratches range in depth from 1 to 50 Å or more. They average around 10-20 Å and have various widths. roughness change induced by etching. For this reason, sections that had no visible scratches were used for RMS quantitative roughness measurements. This procedure was used for quantitative data. Since the 1 x 1 µm sections were subjectively chosen, it was impossible to be sure whether polishing scratches were completely avoided in the RMS roughness measurements. To reduce subjectivity, power spectrum distribution (PSD) data were obtained for each sample. The PSD is based on the entire area of the surface scanned and therefore removes the subjective choice of regions of interest. PSD's were used to verify the RMS trends qualitatively. Figure 18 shows PSD data which are simply intensity vs. wavelength graphs that assigns a "power" to the relative number of occurrences of a feature of a given





Height



Height

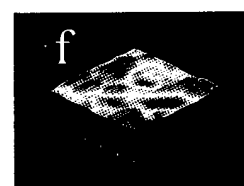
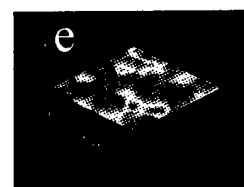
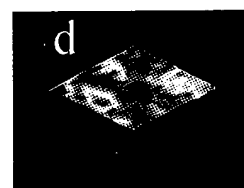


Figure 17. Procedure for determining RMS roughness for a given sample. Two  $10 \times 10 \mu\text{m}$  scans were obtained for each sample. Three to four  $1 \times 1 \mu\text{m}$  sections were chosen from each scan where scratches were minimal. RMS roughness calculations were performed on each of these regions and averaged to get the RMS average roughness for the given sample.

size. Thus fluctuations along the curve are for ridges and valleys that occur more often than other random features. The area under this curve is the RMS roughness for the entire

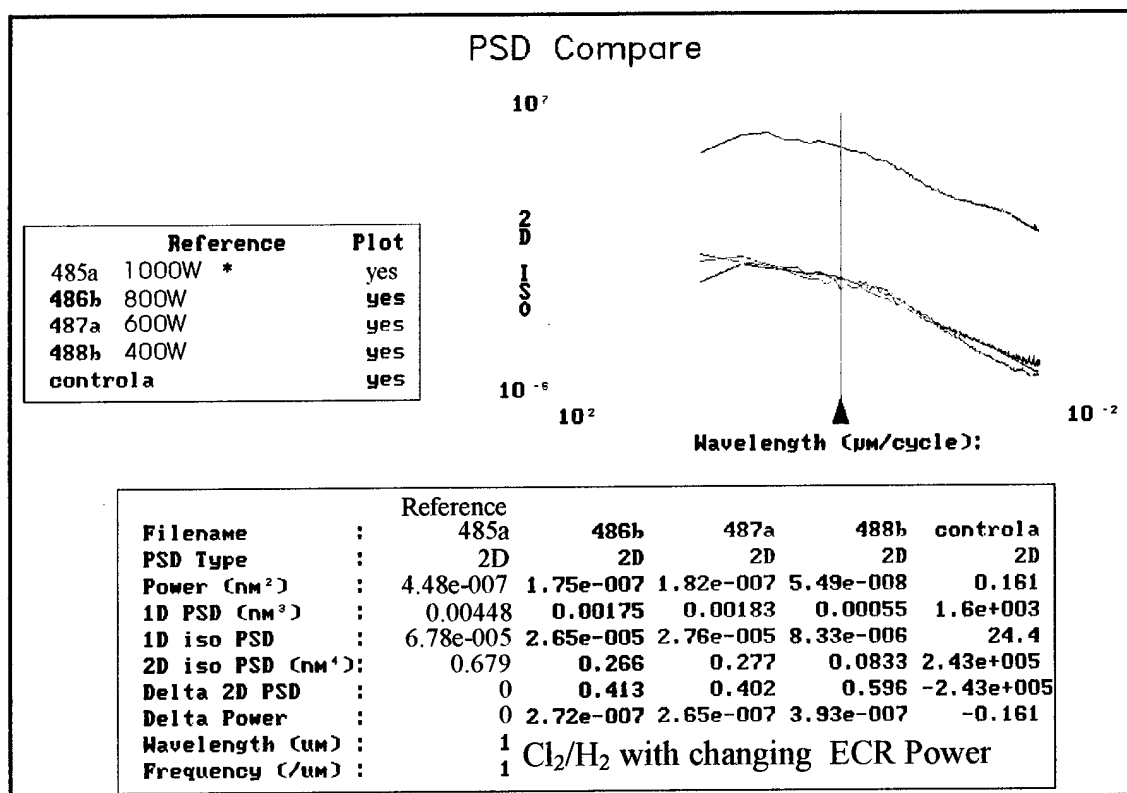
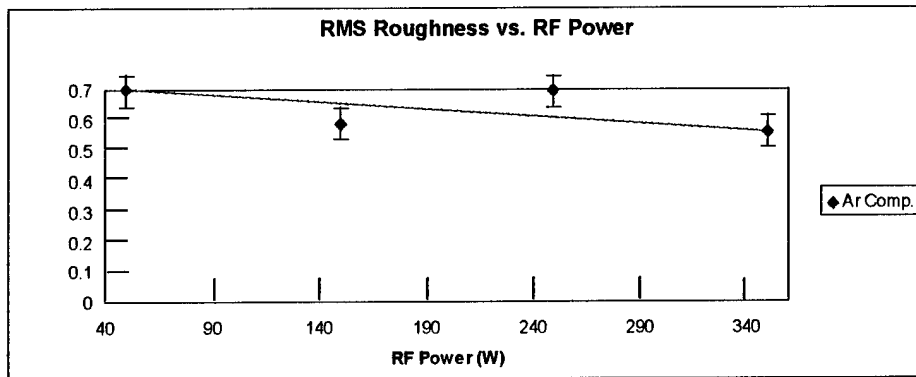


Figure 18. Representative PSD curves comparing roughness for Cl<sub>2</sub>/H<sub>2</sub> plasmas with varying ECR power.

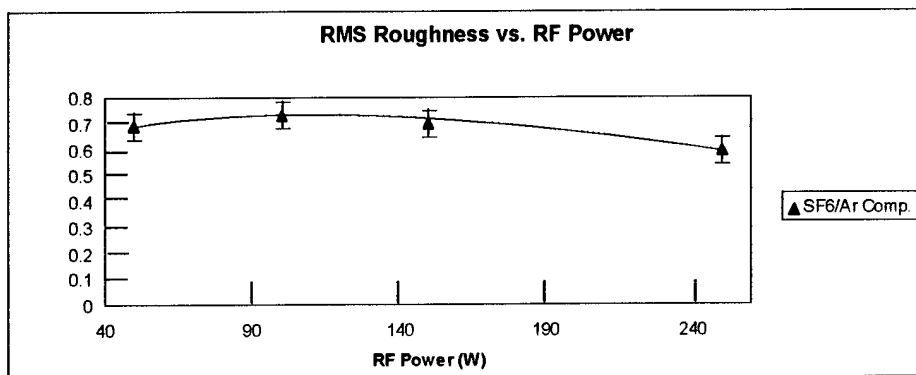
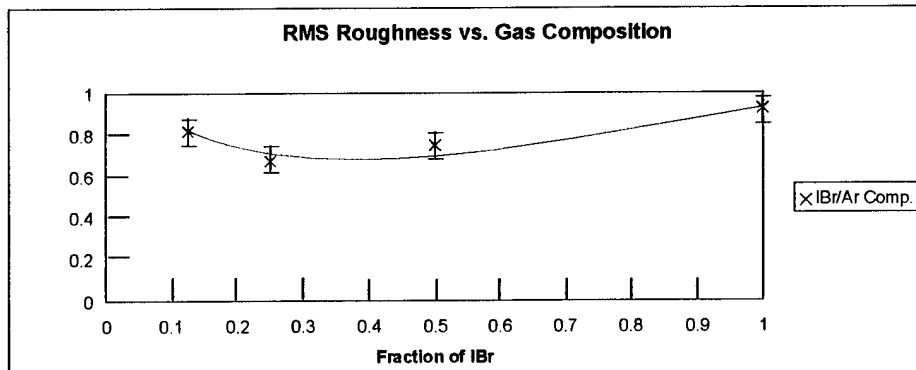
sample. By comparing the general heights of the PSD curves for each sample, a trend can be seen even though the RMS roughness over the entire sample can be highly variable. This helps remove subjectivity from the roughness analysis process. It is only qualitative, but it verifies the results of the other, selected area method. All AFM images are displayed in Appendix A and all PSD curves are displayed in Appendix B.

### 3.2.1 Results

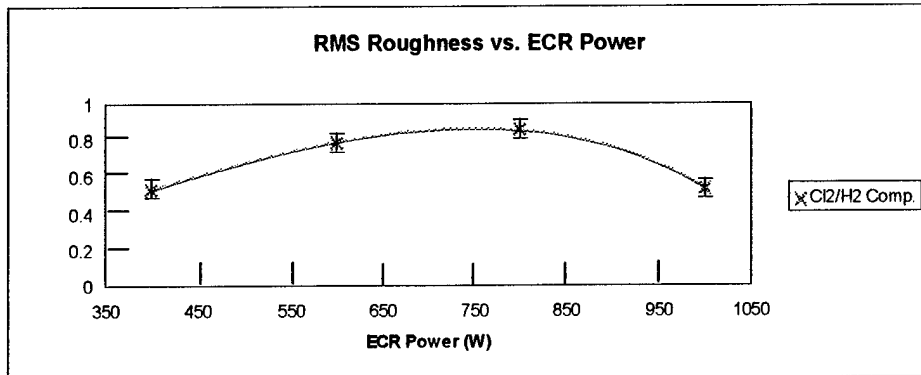
Data for RMS roughness calculations are shown in Figure 19 for the four plasma chemistries.



a) Ar with variable RF power

b) SF<sub>6</sub>/Ar for variable RF power

c) IBr/Ar for variable flow rate of IBr



d)  $\text{Cl}_2/\text{H}_2$  for variable ECR power

Figure 19. Average RMS roughness trends for a) Ar with variable RF power b)  $\text{SF}_6/\text{Ar}$  for variable RF power c)  $\text{IBr}/\text{Ar}$  for variable flow rate of IBr d)  $\text{Cl}_2/\text{H}_2$  for variable ECR power. The dotted lines represent the RMS roughness of the unetched parent sample.

### 3.2.2 Discussion

From the data shown in Figure 19, the surfaces were relatively smooth both before and after etching. Typical tolerances for device fabrication are RMS roughness of 1 nm or less. In each case, the RMS roughness was constant and ranged from 0.6 to 0.8 nm. The standard deviation for the measured average RMS roughnesses was calculated to be 0.1 nm and was used as the error for these data. These conclusions are consistent with the PSD curves. In all cases the surface roughness was either unchanged from the parent, unetched, control sample, or they were reduced by etching. Smoothing can be explained by preferential etching of sharp points. In a plasma etching system, any surface that is sharp cornered or changes abruptly will tend to etch faster than its surroundings because of field curvature near them. Since the parent sample is highly scratched by the polishing process, one would expect a reduction in the surface roughness due to sputtering in the etch process. This is exactly what is observed.

In the PSD for  $\text{SF}_6$ , the 50 Watt and 150 Watt etches showed unchanged roughness while the 100 and 250 Watt etches showed a reduction in roughness. First, the 150 Watt etch rate was anomalously low as described above and shown in Figure 13. It is ignored. The trend then is very clear. The 50 Watt has the highest roughness, the 100 Watt has an intermediate and the 250 Watt has the lowest roughness. Again this is because of the smoothing effect of sputtering on sharp features. One expects higher sputtering to have smoother surfaces overall.

In the PSD for  $\text{Cl}_2/\text{H}_2$ , all curves are approximately reduced by the same amount. This would be expected because in all cases, the RF is unchanged and the sputter component is not significantly altered. Sputtering is lowered somewhat as ECR power increases but not enough to change the surface damage effects.

In the PSD for  $\text{IBr}/\text{Ar}$ , the 0.25 data point is somewhat questionable. Note how it lies considerably below the etch rate best fit curve in Figure 13. This indicates that this particular sample may have been affected in some uncontrollable manner during the etching process. This point is therefore ignored. Notice that the 0.125 curve has a higher roughness slightly than the 0.5 curve. This makes sense from the argument given earlier that iodine and bromine ions are simply too massive to impart any energy to the surface for sputtering. They are involved with elastic collisions. The trend then would suggest that the curve for pure iodine bromide should have the highest roughness because there should be little sputter smoothing. This is not the case. What is observed may possibly be explained by the reactivity of the bromine and iodine. Perhaps they chemically etched the surface in a preferential manner that lowered the roughness. This cannot be verified. It is an anomaly with respect to the rest of the data observed.

Finally, in the PSD comparing chemistries, iodine bromide and sulfur hexafluoride have the highest surface roughness. This makes sense because the massive molecules will not participate in sputtering. IBr/Ar is rougher than SF<sub>6</sub> because even its fully dissociated species will not sputter. SF<sub>6</sub>'s constituents will sputter so it is lower in surface roughness. Cl<sub>2</sub>/H<sub>2</sub> and argon both have significantly reduced roughnesses because all species will etch the surface by sputtering.

In the PSD for argon plasmas with changing RF power, all etched surface roughnesses were lower than the parent sample. As discussed above, sputtering should smoothen the surfaces.

### 3.3 AES

#### 3.3.1 AES Results

AES was used to determine the surface composition for each of the 6H SiC samples. Surface survey and depth profiles were obtained using a 5.0 kV primary electron beam. Sputtering time was 5 min for all scans. Factors affecting termination of the

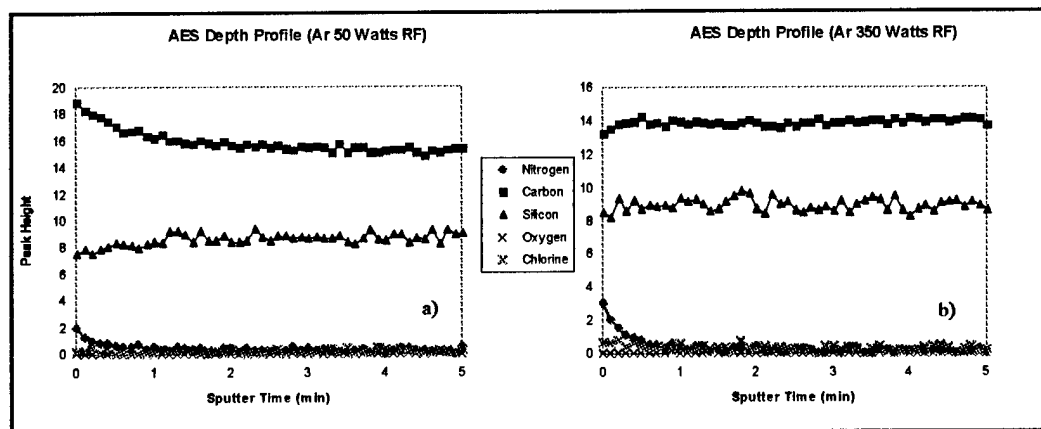


Figure 20. AES depth profiles for argon plasmas with 1000 Watts ECR power, 1.5 mTorr total pressure, 15 sccm flow rate, and a) 50 Watts RF power and b) 350 Watts RF Power.

plasma plus ion implantation. Comparisons are drawn between samples within each gas chemistry for contamination and termination of the SiC surface.

After argon plasma treatment, the depth profiles shown in Figure 20 were found. For this experiment, the RF bias effects on the depth profile were investigated.

Sulfur hexafluoride plasmas resulted in the AES depth profiles in Figure 21. For this experiment, the RF bias effects on the depth profile were investigated for a gas chemistry that had a chemically reactive component.

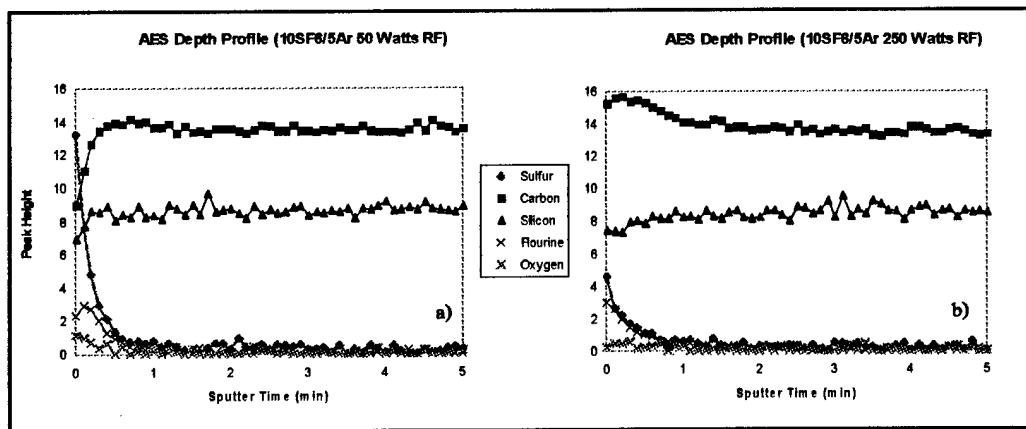


Figure 21. AES Depth profiles for sulfur hexafluoride plasmas with 1000 Watts ECR power, 1.5 mTorr total pressure, 0.667 active flow rate to total flow rate ratio, and a) 50 Watts RF power and b) 250 Watts RF Power.

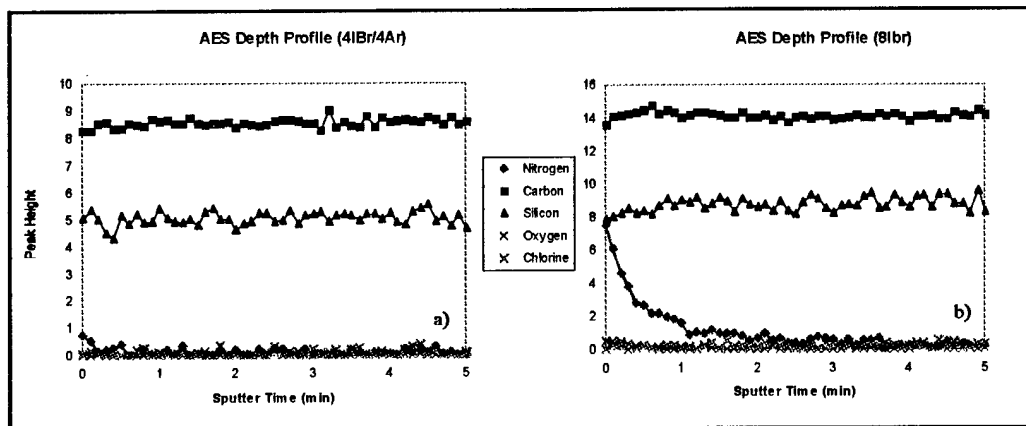


Figure 22. AES Depth profiles for iodine bromide plasmas with 1000 Watts ECR power, 1.5 mTorr total pressure, 150 Watts RF power and a) 0.5 active flow rate to total flow rate ratio and b) Pure IBr at a flow rate of 8 sccm.

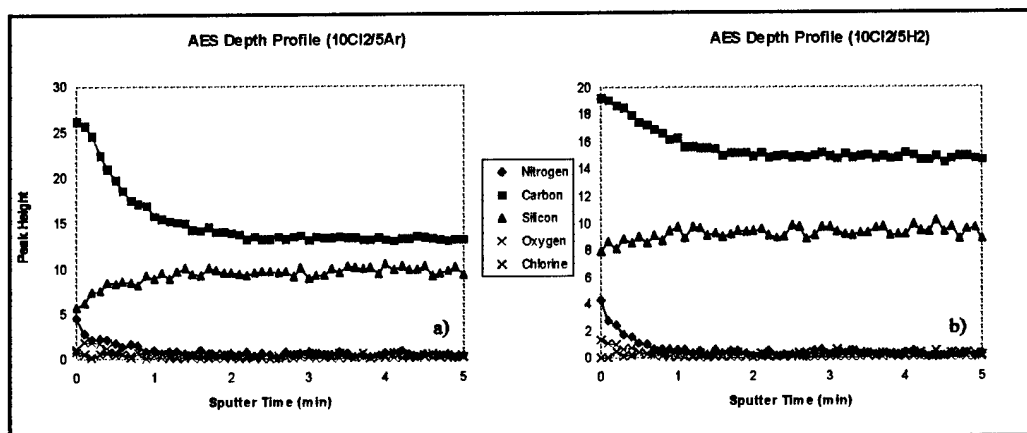


Figure 23. AES Depth profiles for chlorine plasmas with 1000 Watts ECR power, 1.5 mTorr total pressure, 0.667 active flow rate to total flow rate ratio, 150 Watts RF power, and a) argon as the carrier gas or b) hydrogen as the carrier gas.

Iodine bromide plasmas resulted in the depth profiles in Figure 22. For this experiment, the effect of the ratio of active species flow rate to total flow rate was studied.

Chlorine plasmas resulted in the depth profiles in Figure 23. For this experiment, the effect of carrier gas was examined.

### 3.3.2 AES Discussion

#### 3.3.2.1 Argon etches

In the experiments with argon plasmas, it was shown that for low RF biases, there was a carbon terminated surface. In the unetched control parent sample, the wafer had a silicon terminated surface as reported by Cree Research and verified by the AES depth profile in Figure 24. The change in termination can be explained by the difference in sputtering yields of native carbon and silicon. Carbon etches very slowly with respect to silicon. This difference in sputter yields forced carbon to enrich the surface so that the flux of material leaving the surface was stoichiometric, i.e. 50% carbon and 50% silicon.<sup>12</sup>



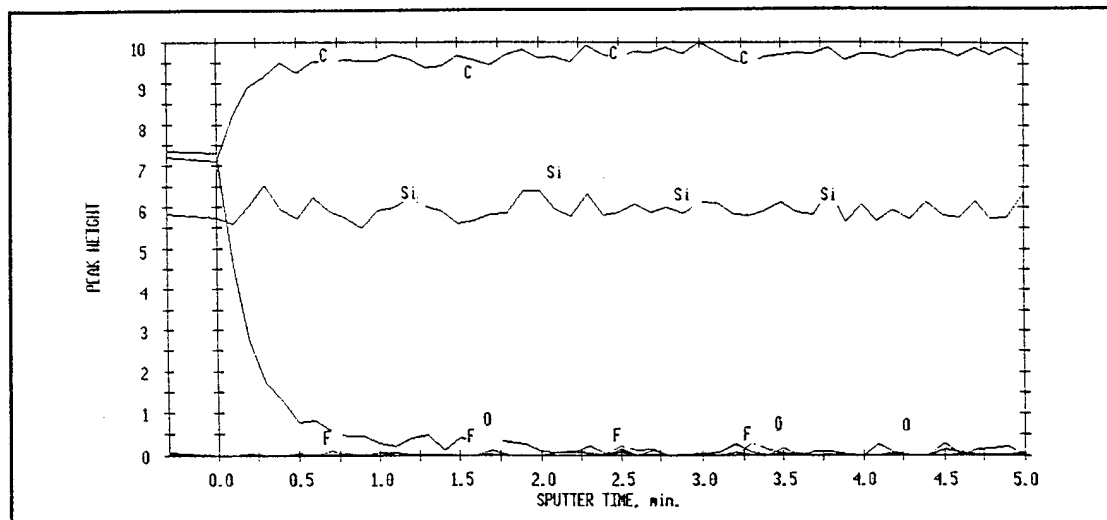


Figure 24. AES depth profile for the parent, unetched control sample indicating the carbon depleted and silicon terminated surface.

This difference in sputter yields for argon is verified by Table 7. The sputter yield for silicon based on mass matching alone is over 10 times better than for carbon. In the sample with extremely high RF bias, the surface was stoichiometrically terminated and neither element was favored. This may denote that the sputtering of the surface was rapid enough that carbon migration was not necessary to yield stoichiometric fluxes. If this hypothesis is true, even in a plasma with chemically reactive species at high RF powers, the surface should tend toward stoichiometric termination because surface reactions don't have time to take place before sputtering occurs. So volatility of the etch products would not affect the surface termination. To examine this, sulfur hexafluoride was studied.

#### 3.3.2.2 Sulfur hexafluoride etches

Low RF biases resulted in a silicon terminated surface for sulfurhexafluoride plasmas. Sulfur and fluorine contaminated the surface to a depth of a few angstroms. Since volatility of the etch products was a factor, Table 8 shows the volatilities of some

of the etch species expected in this experiment. The volatility of carbon tetrafluoride is almost twice that of silicon tetrafluoride. Because of this, carbon was preferentially etched in the plasma with low RF biases where surface chemical reactions were expected to be dominant. The  $\text{CF}_4$  should have volatilized much more quickly than  $\text{SiF}_4$ . This was verified by the silicon terminated and heavily carbon depleted surface with the fluorine contaminant presumably being present as  $\text{SiF}_4$ . With increased RF biases, sputtering effects begin to dominate and the volatility becomes less of an important factor. The

Table 8. Volatilities of several expected etch products for  $\text{SF}_6/\text{Ar}$  chemistries. Free energy of formation for all species indicate that they will spontaneously form.<sup>15</sup>

Etch Product for $\text{SF}_6$	Temperature (K) to reach VP of 1 mT	Temperature (K) to reach VP of 10 mT	Gibbs Formation Energy at 298 K
$\text{CF}_4$	88.4	103.7	-210
$\text{SiF}_4$	129	142.6	-375
$\text{SF}_6$	140.3	158.3	-264.2

surface was being sputtered so much that the reactions were being hindered and sputter dominant etching was occurring. This caused the carbon terminated surface that was seen at the moderate RF of 250 Watts. As Table 7 indicates, the sputter yield of carbon and silicon is almost equal for fluorine ions, however for the sulfur ions, silicon is preferentially etched by a factor of almost 100. There is not a largely carbon terminated surface because there are six times as many fluorine ions as sulfur ions available with argon to sputter the surface. Because of the low fraction of sulfur in the plasma, the extremely high preferential sputtering rate is masked by the similar sputter rates for fluorine. With a further increase in RF, one would expect stoichiometric termination of the surface as was seen at 350 Watts with argon.

### 3.3.2.3 Iodine bromide etches

In experiments with IBr/Ar, there was no change in the depth profiles noted. This was expected since the only etch product that might form,  $\text{CBr}_4$ , was highly volatile and the likelihood of formation was low because the Gibbs free energy of formation was positive. Table 9 shows the volatility of the etch species expected in this experiment. Energy would be required to form this species since it does not spontaneously form. There are no data for lower pressures but one can assume the temperature for creating 1

Table 9. Volatility of the expected etch product for IBr/Ar chemistries. Free energy of formation indicates that this species will not spontaneously form.<sup>15</sup>

Etch Product for IBr	Temperature (K) to reach VP of 1 mT	Temperature (K) to reach VP of 10 mT	Temperature (K) to reach VP of 40 mT	Gibbs Formation Energy at 298 K
$\text{CBr}_4$	N/A	N/A	369.3	4.873

milliTorr is significantly lower than 369.3 K if energy is supplied for this etch product to form. Thus there should be no preferential etching of either silicon or carbon.

Interestingly, the surface of SiC etched with IBr/Ar was not carbon terminated even though the RF bias was low at 150 Watts. This may be because there was a lower volatility for silicon tetrabromide forcing silicon to remain on the surface more than it normally would. The actual volatility for this species could not be found so it is uncertain if this is a correct assumption.

Also it should be noted that the sputtering effect should be drastically reduced in both cases because of the mismatch of the mass of the ions with Si and C. Collisions were completely elastic for iodine and bromine ions so in the experiment with 50% IBr and 50% argon, argon ion density was low and iodine and bromine ions didn't contribute much to sputtering. Those argon ions available for sputtering were hindered by iodine and bromine ions such that the carbon didn't need to migrate to the surface to enhance the

stoichiometric sputter fluxes. Table 7 confirms that there is no preference in sputter yields for carbon or silicon with iodine and bromine ions. In the case of a ratio of 1, there were no ions that could sputter effectively so a stoichiometric terminated surface, as the one observed, would be expected.

#### 3.3.2.4 Chlorine etches

Volatility was a large factor in experiments with chlorine gas chemistries. Table 10 shows the volatilities of the etch species expected in this experiment. In the  $\text{Cl}_2/\text{Ar}$  plasma, the surface was highly carbon enriched and significantly silicon depleted. This makes sense because the volatility of carbon tetrachloride is lower than silicon

Table 10. Volatilities of several expected etch products for  $\text{Cl}_2/\text{Ar}$  and  $\text{Cl}_2/\text{H}_2$   $\text{SF}_6/\text{Ar}$  chemistries. Free energy of formation for all species except silane indicate that they will spontaneously form. Silane will not.<sup>15</sup>

Etch Product for $\text{Cl}_2/\text{Ar}$	Temperature (K) to reach VP of 1 mT	Temperature (K) to reach VP of 10 mT	Gibbs Formation Energy at 298 K
$\text{Cl}_2$	155	171.4	
$\text{SiCl}_4$	209.6	238.6	-147.47
$\text{CCl}_4$	223	253.4	-14.49

Etch Product for $\text{Cl}_2/\text{H}_2$	Temperature (K) to reach VP of 1 mT	Temperature (K) to reach VP of 10 mT	Gibbs Formation Energy at 298 K
$\text{CH}_4$	67.1	77.5	-12.13
$\text{SiH}_4$	93.7	110	13.6
$\text{Cl}_2$	155	171.4	

tetrachloride. Silicon was preferentially etched away leaving carbon enriched and silicon depleted surfaces. There was enhanced sputtering because all species had a good mass match for inelastic collisions. This resulted in larger migration of carbon to the surface as it does in pure argon etches. Table 7 indicates that chlorine sputter yields for silicon are 20 times larger than for carbon. The combined preferential etching of silicon by chlorine

and argon and gives rise to the high carbon termination in the plasmas with argon as the carrier. In plasmas with hydrogen as the carrier, the carbon termination is reduced because hydrogen does not preferentially etch carbon or silicon according to the values in Table 7. The results expected are what are observed.

In the  $\text{Cl}_2/\text{H}_2$  plasma, the surface was still carbon enriched but not as much, and the silicon was only lightly depleted. In this case, the volatility of methane and silane are much much greater than the chlorides so they would be expected to leave the surface. Hydrogen, however, is known as a passivating substance and instead of breaking bonds within the surface of the SiC to liberate either a Si or C atom, it simply reduced the energetically unfavorable broken surface bonds. A "protective" layer was created on the surface that prevented chlorine diffusion into the lattice. This reduced the overall chemical etching rate. Thus what was seen was a weaker version of the  $\text{Cl}_2/\text{Ar}$  plasma effects. This was what was expected and observed.

## CHAPTER 4 CONCLUSIONS

The objectives of this research were: 1) to investigate different gas mixture combinations for high density ECR plasma etching of SiC, 2) to determine finite etch rates for the various gas combinations as a function of ECR power, RF power, chamber pressure, and flow rate ratio of active species to carrier species, 3) to quantify damage in surface morphology in 6H-SiC after etching using AFM, and 4) to analyze surface composition for etchant residues and C or Si termination after etching. The following conclusions were drawn from this research.

Each of the plasmas combined a sputter etchant carrier gas, usually argon, and a highly reactive halogenated species for chemical etching. A series of etches were performed with pure argon to distinguish between pure sputtering and to determine any synergistic effects of adding reactive gases. For any given univariant system, there should be an etch rate curve that resembles Figure 8 where the etch rate is low for either pure sputtering or pure chemical reactions, but high when both sputtering and plasma activation of the gas phase molecules are used. Only a fraction of the curve will be determined if the full range of the variables are not investigated. For the gas mixtures studied, Figure 25 summarized the portion of the ideal etch rate curve that was observed for the range of variables studied. All of the gas mixtures favored the chemically dominant side of the etch rate curve for the given parameters. Chlorine, under the current range of experimental

parameters, had the largest range of etch rates along the ideal etch curve. Mixtures of  $\text{SF}_6/\text{Ar}$  resulted in the highest etch rates except in plasmas with ECR power greater than









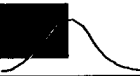




Plasma	ECR	RF	Pressure	Active Fraction
$\text{Cl}_2/\text{H}_2$	1800-1200-800 			
$\text{Cl}_2/\text{Ar}$	800-2600 	0-2500-800 		1000-825 
$\text{IBr}/\text{Ar}$	1000-800 	100-1000 		700-600 
$\text{SF}_6/\text{Ar}$	1300-2000 	2100-2600 	1250-3900 	
Ar	550-800 	800-600 	800-750 	

Figure 25. Portion of the theoretical etch rate curve that each gas chemistry belongs to under the range of conditions studied. The etch rate ranges are shown in  $\text{\AA}/\text{min}$  for each chemistry. The axis for the theoretical curve is EP as shown in Figure 8.

650 Watts. For ECR power  $> 650$  W.,  $\text{Cl}_2/\text{Ar}$  mixtures had the largest etch rates. Because similar masses for the gas and substrate led to high sputter rates, and fluorine was highly reactive. Other than for ECR power  $> 650$  W.,  $\text{Cl}_2/\text{Ar}$  had the second largest etch rate in all experiments. The etch rates for  $\text{Cl}_2/\text{H}_2$  mixtures were third largest. The reduction in etch rate for  $\text{Cl}_2/\text{H}_2$  was thought to be due to passivation of damaged surfaces by hydrogen and due to the loss of extra sputtering that was previously available from argon ions. Finally  $\text{IBr}/\text{Ar}$  had the lowest etch rate of the gas mixtures studied, exceeding

only pure argon. The low rate for IBr/Ar results from low sputtering rates due to mismatched masses between the etchant gases and SiC.

AFM studies revealed in all cases, reduction in the surface roughness for etched versus unetched samples. This conclusion was supported through the use of power spectrum density (PSD) curves. The smoothest surfaces were found after etches at high RF powers, very low or very high ECR powers, and moderate ratios of reactive to carrier gas flow rates. The dependence of roughness on these parameters was very small however, and all conditions resulted in smooth surfaces with RMS roughnesses on the order of 0.6 to 0.8 nm. The acceptable roughness range for semiconductor device preparation is typically 1 to 2 nm, so all of the etchant species studied would be acceptable for SiC device patterning.<sup>14</sup>

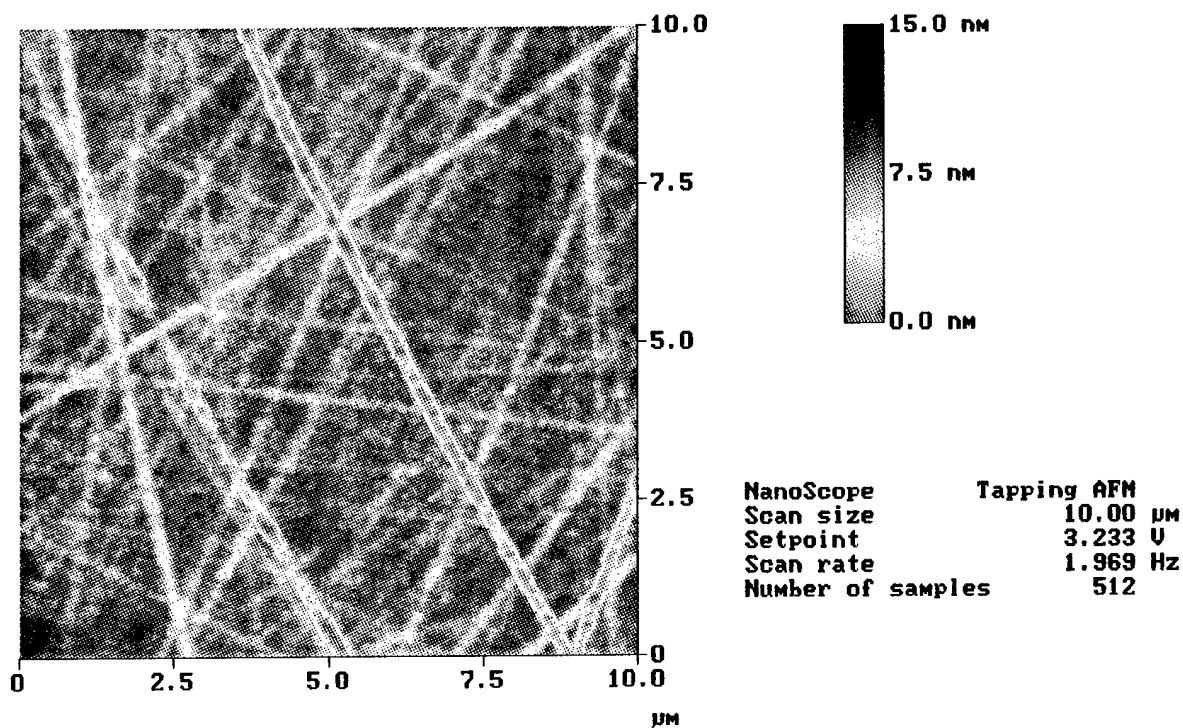
Auger electron spectroscopy data showed that there was little contamination of the surface in most cases due to etch products and often etching resulted in carbon enriched surfaces. Silicon was depleted on the surface of samples etched in low RF power argon, low and high RF power SF<sub>6</sub>/Ar, and at high reactive species concentrations of Cl<sub>2</sub> (10 sccm Cl<sub>2</sub> to 5 sccm Ar). Stoichiometric terminations of Si and C were found with all IBr/Ar or with Ar at high RF powers. All gas mixtures studied exhibited stoichiometric termination at the highest RF powers (>250 Watts). Finally, carbon and silicon depleted surfaces were detected with SF<sub>6</sub>/Ar plasmas at low RF power. Carbon enriched surfaces were detected for high RF power SF<sub>6</sub>/Ar and this gas mixture was the only chemistry which left the surface contaminated with etchant gas. Small concentrations of S and F were detected.



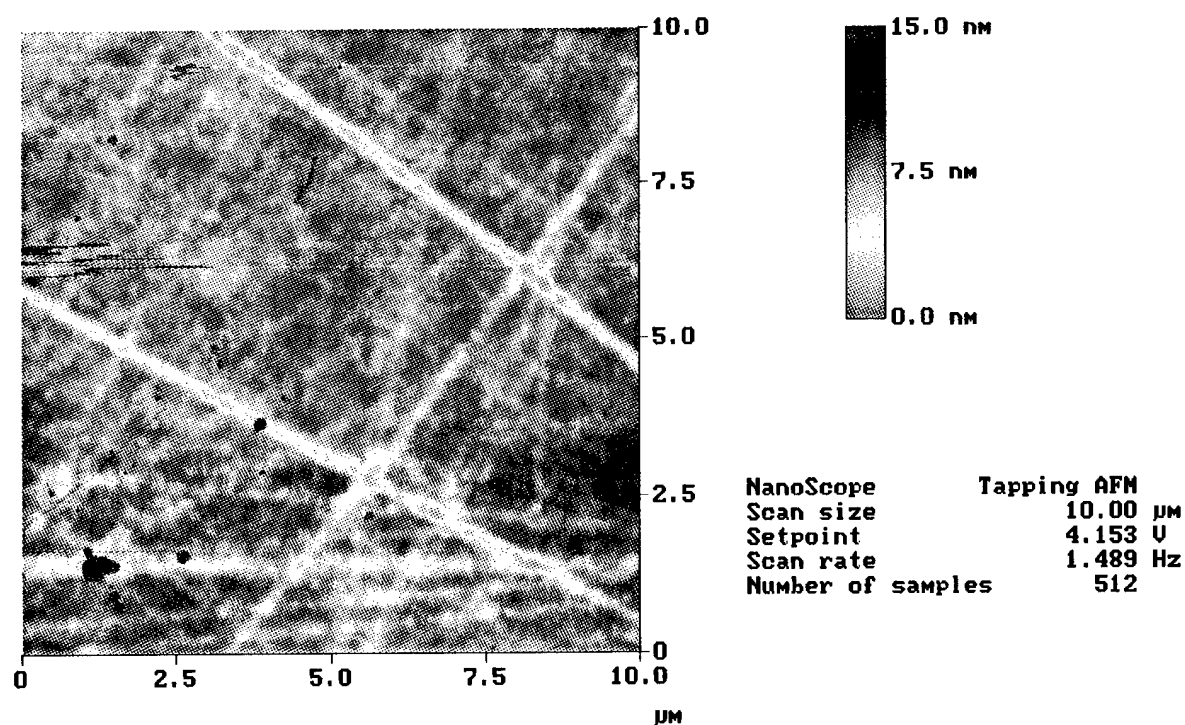
In this study, there are several areas for future research. First, as noted previously, there are several questionable data points. These tests should be performed again to verify that the current questionable data are not correct. Secondly, the expected follow on to a surface analysis study is the actual patterning of surfaces. An important study would test each of the gases studied for mask undercutting under the series of conditions used thus far. A study of this kind would show the chemical nature of each of the plasma mixtures more clearly. One final study would involve electronic measurements of the damage associated with etching due to surface reconstruction and implantation of etchant species.

Applications of the plasma etching techniques provide an abundance of areas for future work, particularly in the area of device fabrication. After surfaces are patterned, metal contacts must be applied to the surface for device fabrication. There are several areas for improvement in determining adequate ohmic contacts to SiC. While finding an ohmic contact is not difficult, finding one that is resistant to the temperatures in which SiC is expected to operate is a puzzle even today. Diffusion barrier studies are currently underway. In addition, to reduce resistivity of the interface, heterostructure contacts are being investigated. Clearly, there are several directions that research may go which would benefit from the techniques studied.

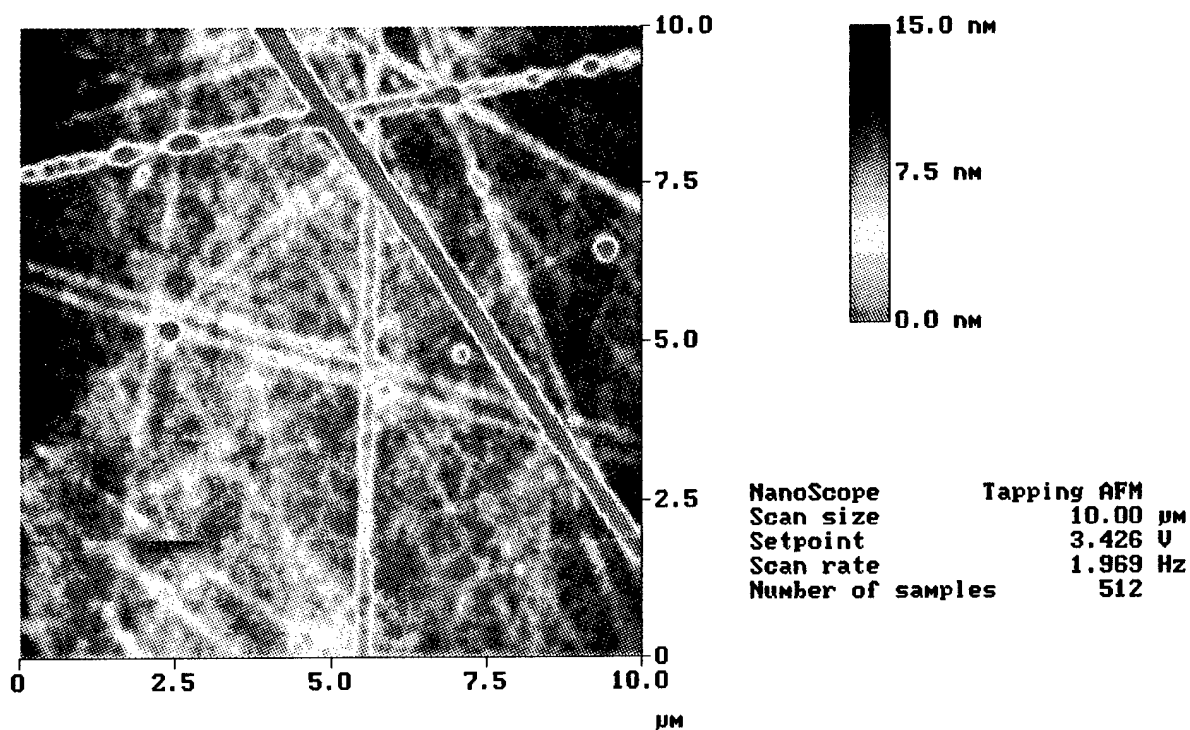
**APPENDIX A**  
**ATOMIC FORCE MICROSCOPY IMAGES**



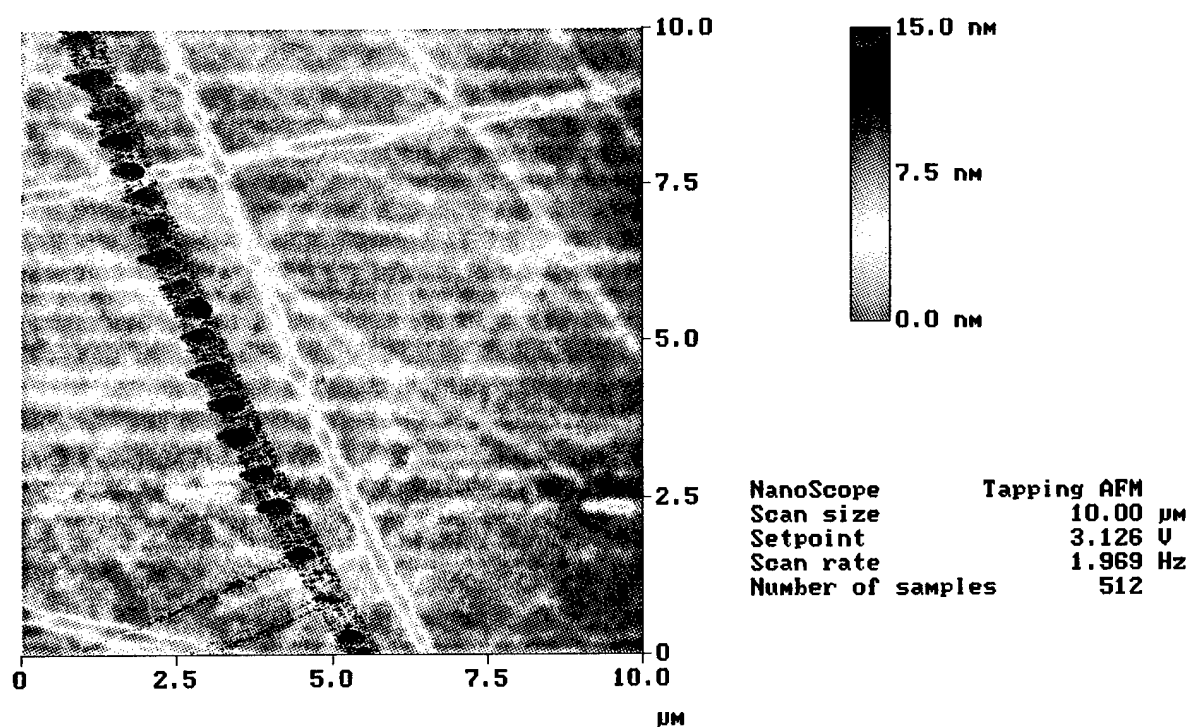
A-1 Argon with 50 W RF power, 1000 W ECR power, and 1.5 mTorr.



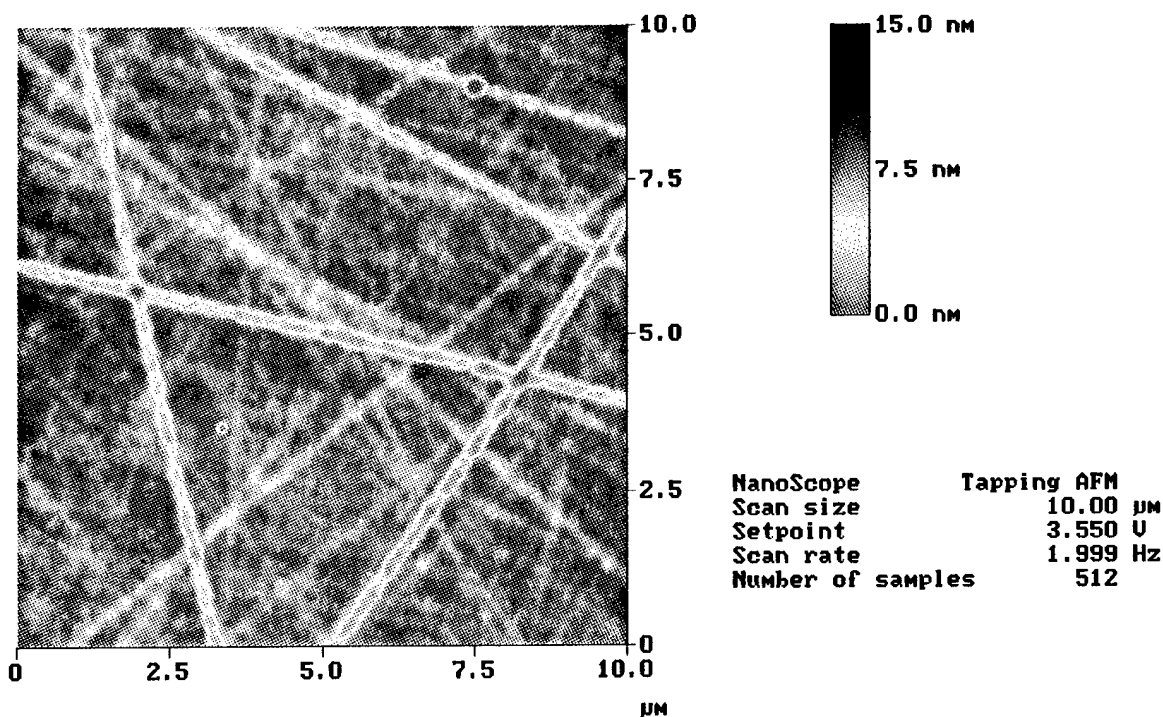
A-2 Argon with 150 W RF power, 1000 W ECR power, and 1.5 mTorr.



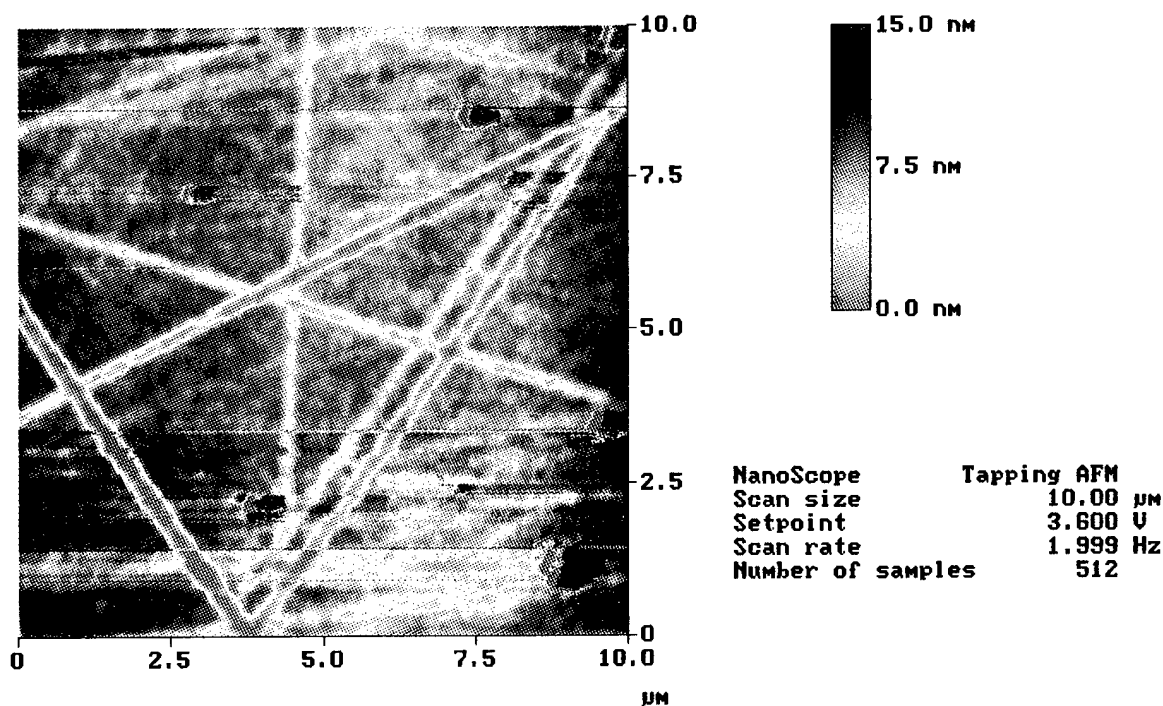
A-3 Argon with 250 W RF power, 1000 W ECR power, and 1.5 mTorr.



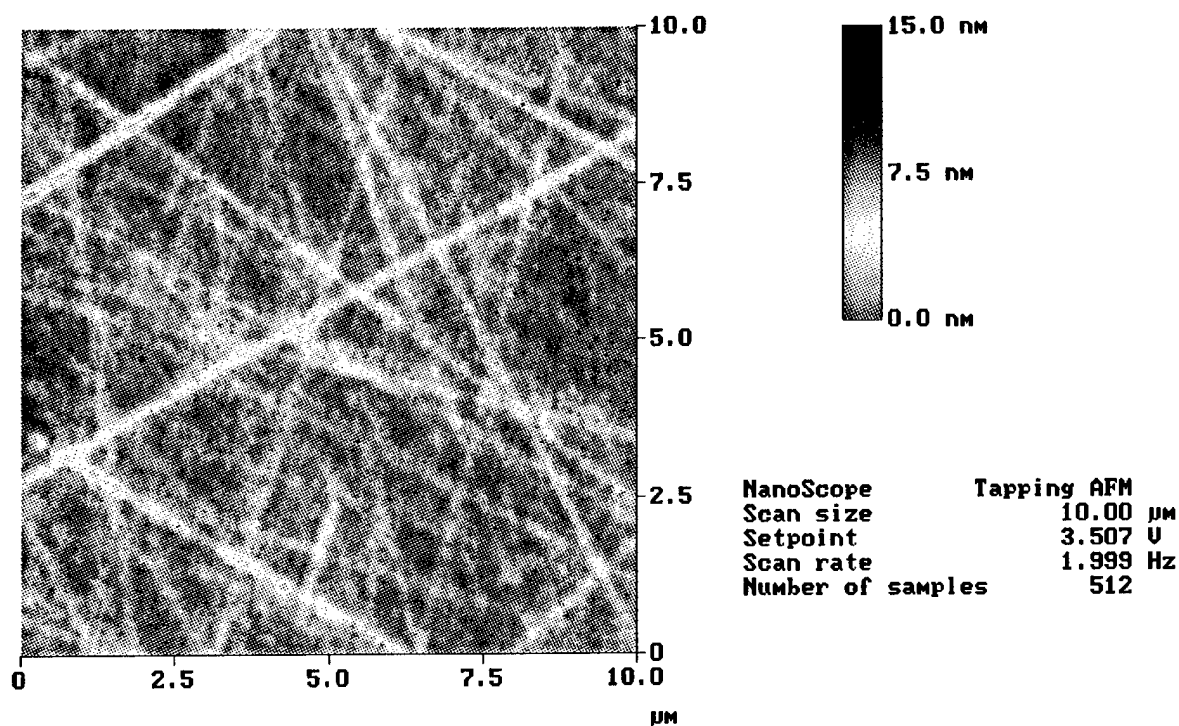
A-4 Argon with 350 W RF power, 1000 W ECR power, and 1.5 mTorr.



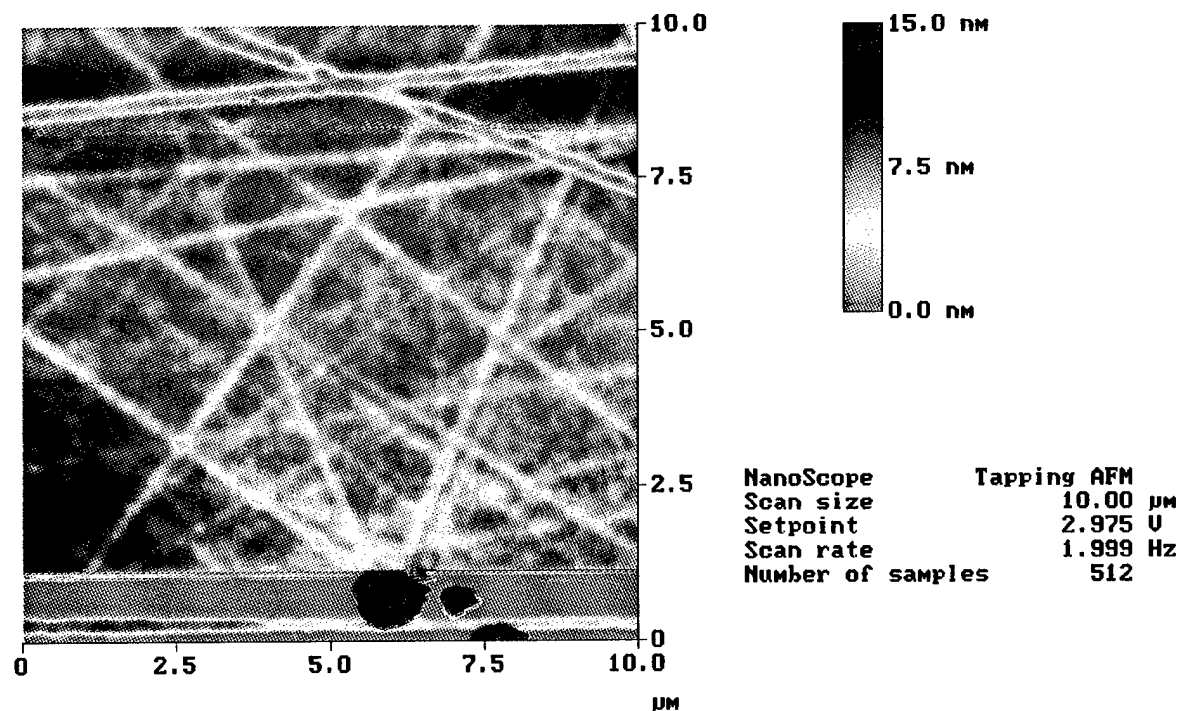
A-5 SF<sub>6</sub>/Ar with 50 W RF power, 1000 W ECR power, 1.5 mTorr, and 0.667 active fraction.



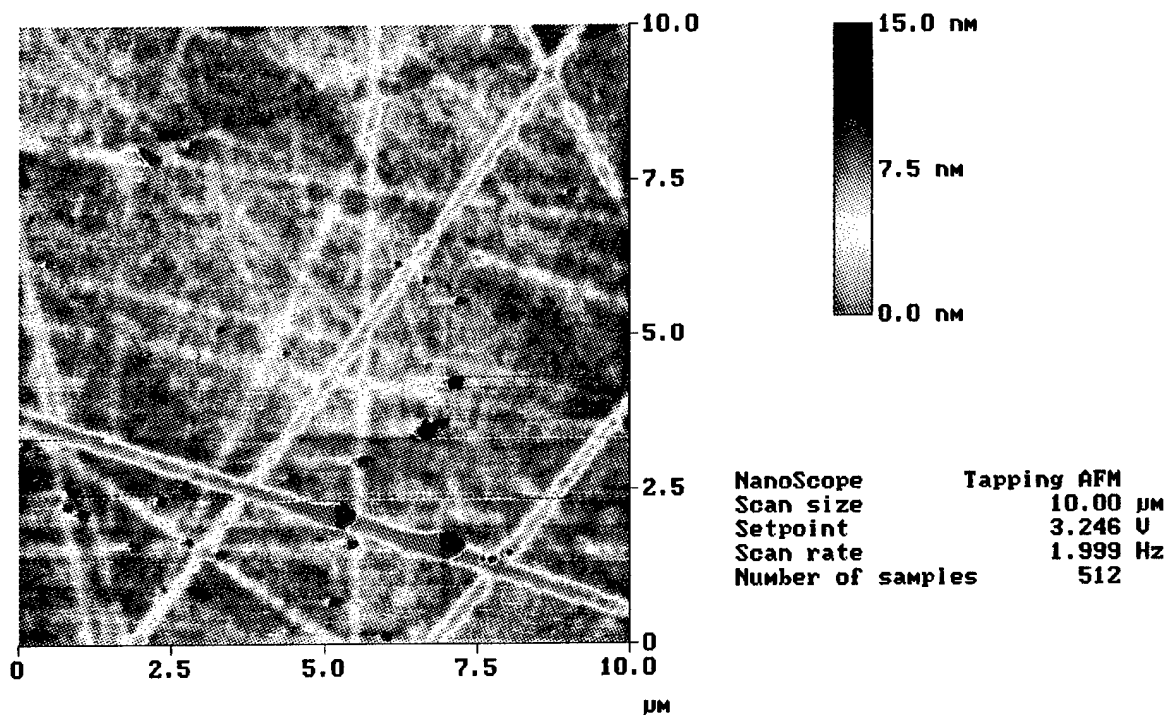
A-6 SF<sub>6</sub>/Ar with 100 W RF power, 1000 W ECR power, 1.5 mTorr, and 0.667 active fraction.



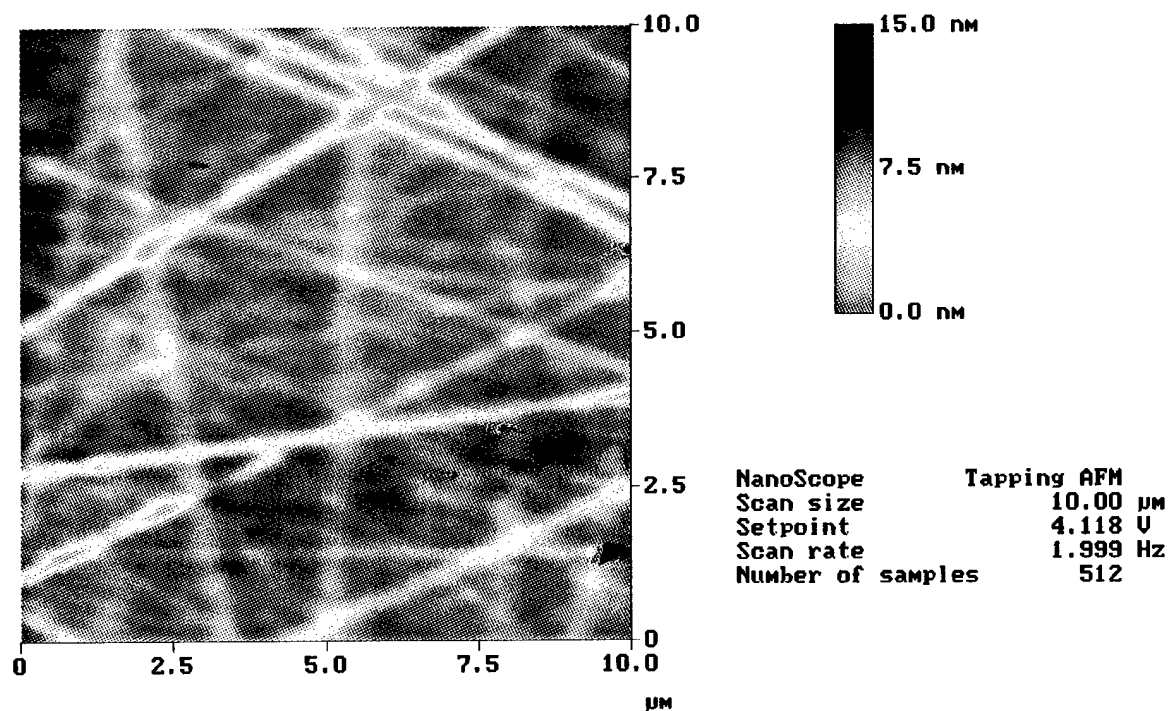
A-7 SF<sub>6</sub>/Ar with 150 W RF power, 1000 W ECR power, 1.5 mTorr, and 0.667 active fraction.



A-8 SF<sub>6</sub>/Ar with 250 W RF power, 1000 W ECR power, 1.5 mTorr, and 0.667 active fraction.

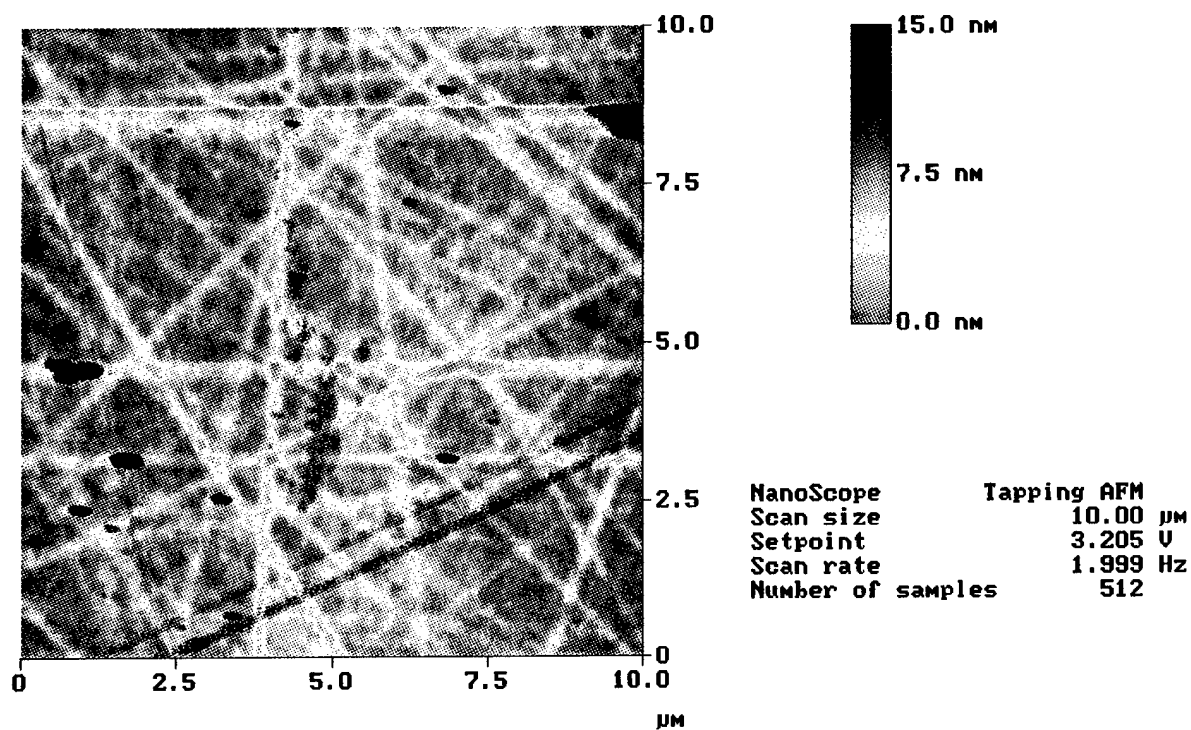


A-9 IBr/Ar with 150 W RF power, 1000 W ECR power, 1.5 mTorr, and 0.125 active fraction.

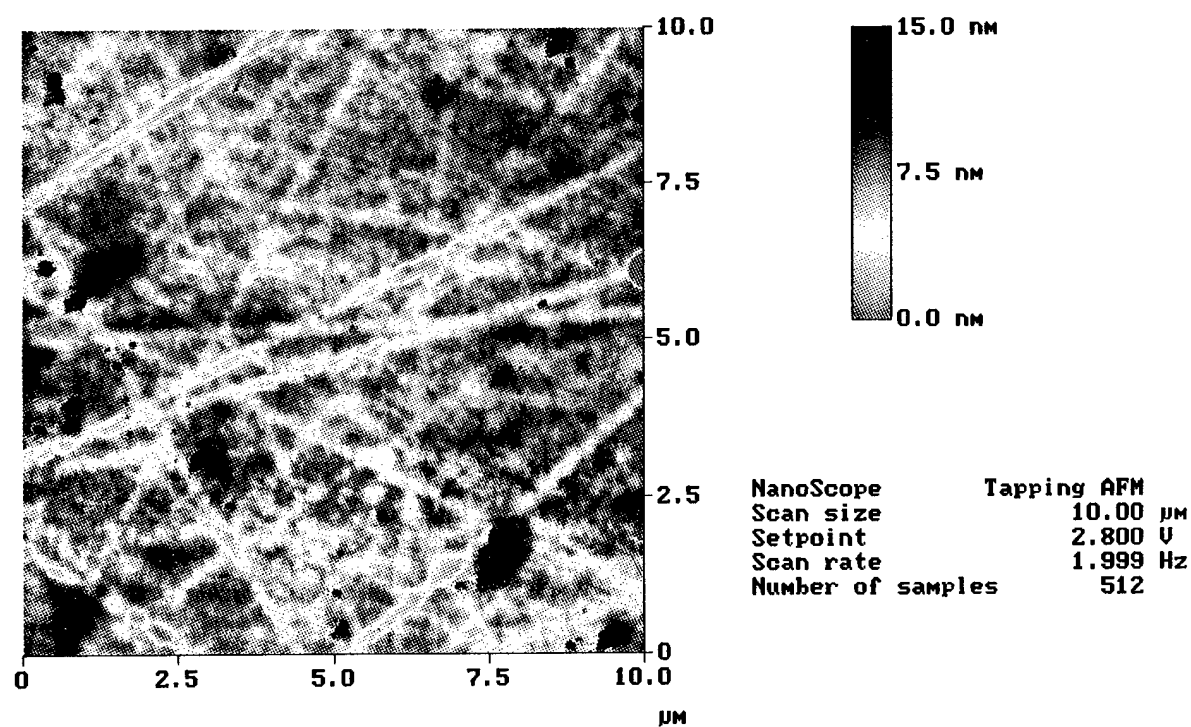


A-10 IBr/Ar with 150 W RF power, 1000 W ECR power, 1.5 mTorr, and 0.25 active fraction.



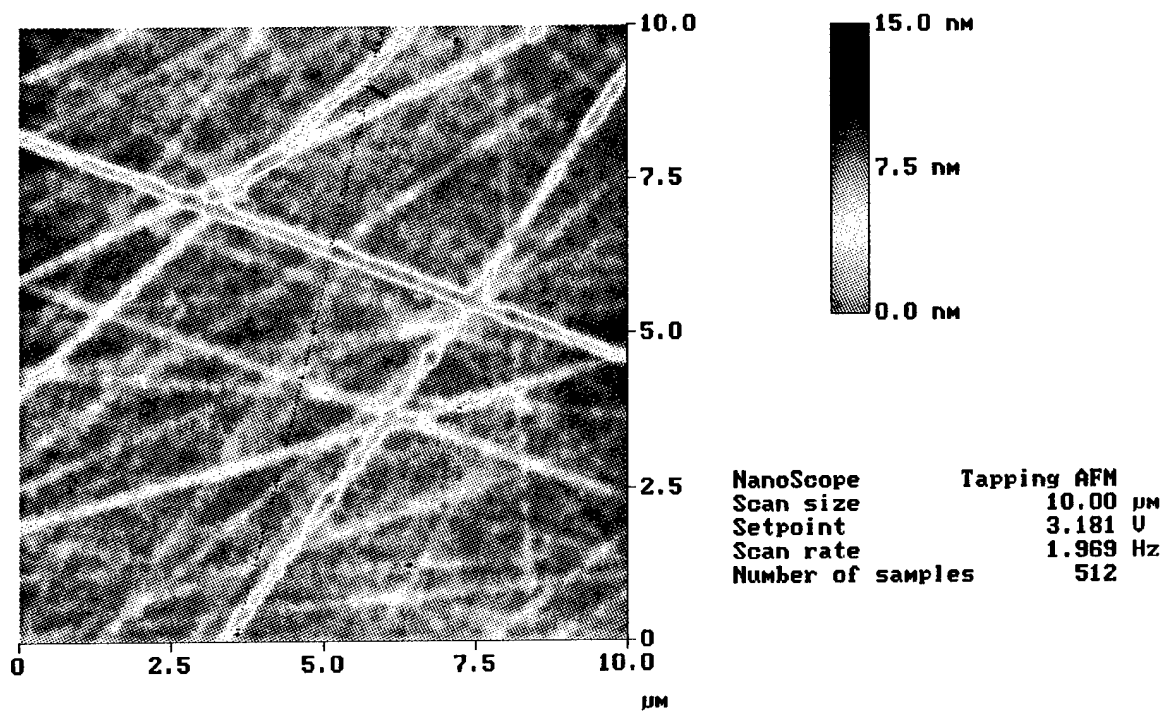


A-11 IBr/Ar with 150 W RF power, 1000 W ECR power, 1.5 mTorr, and 0.5 active fraction.

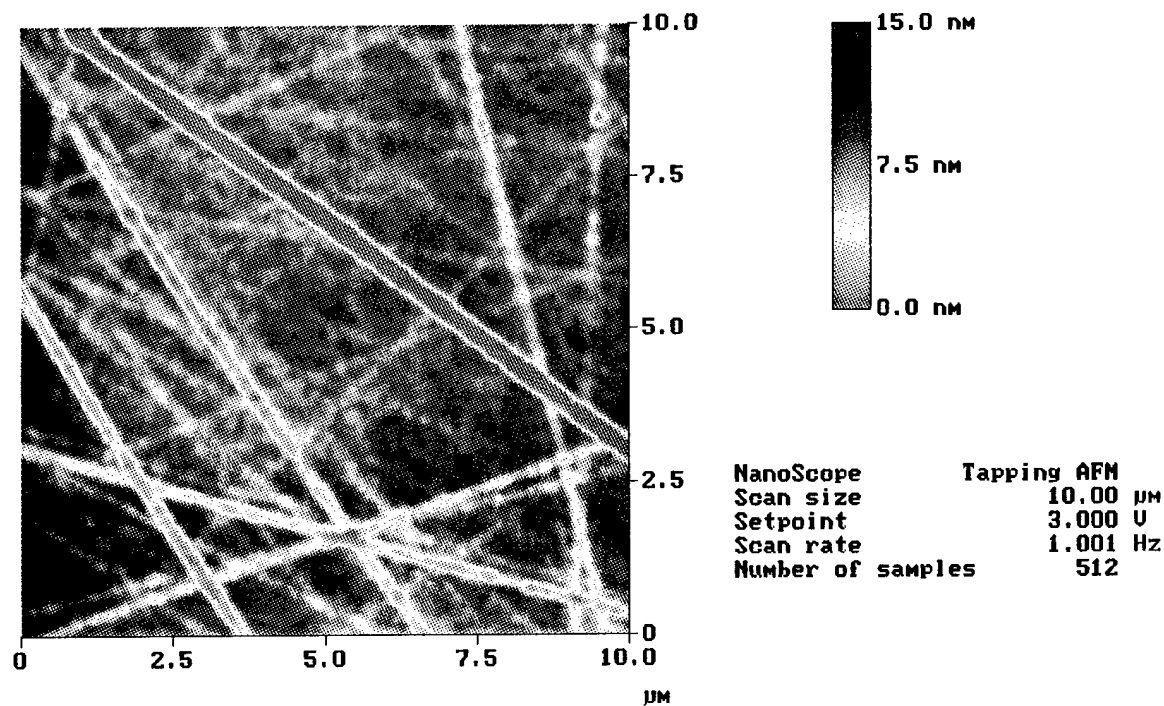


A-12 IBr/Ar with 150 W RF power, 1000 W ECR power, 1.5 mTorr, and 1.0 active fraction.

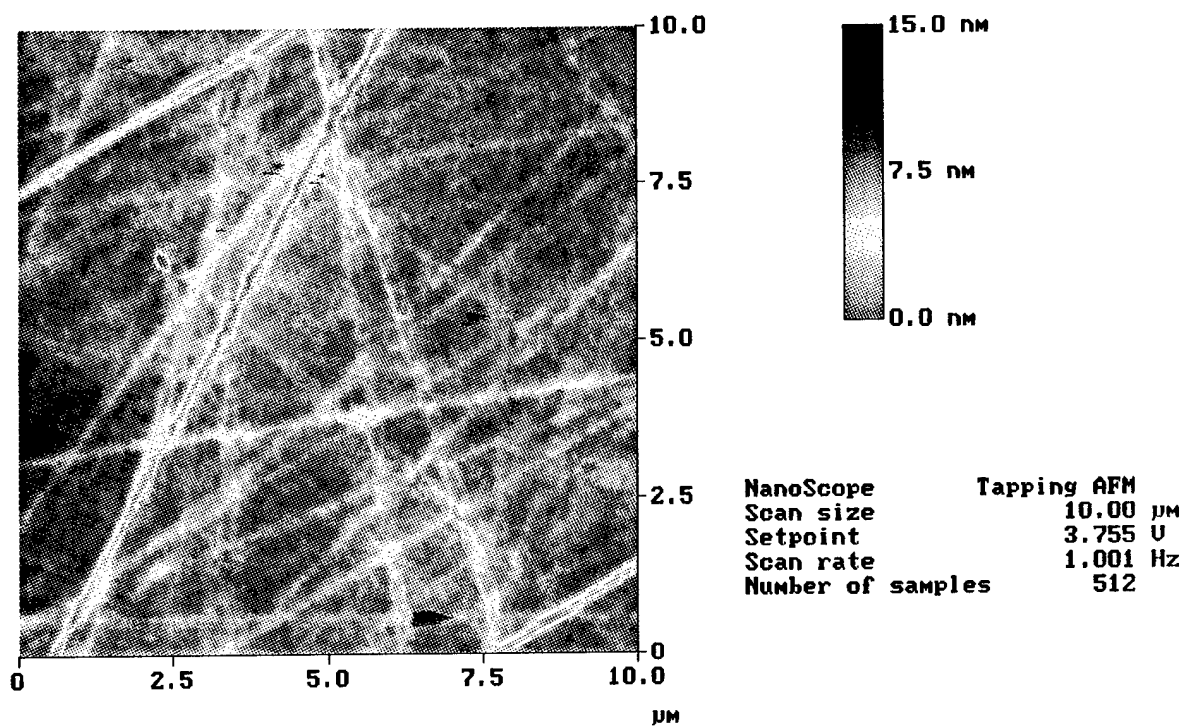




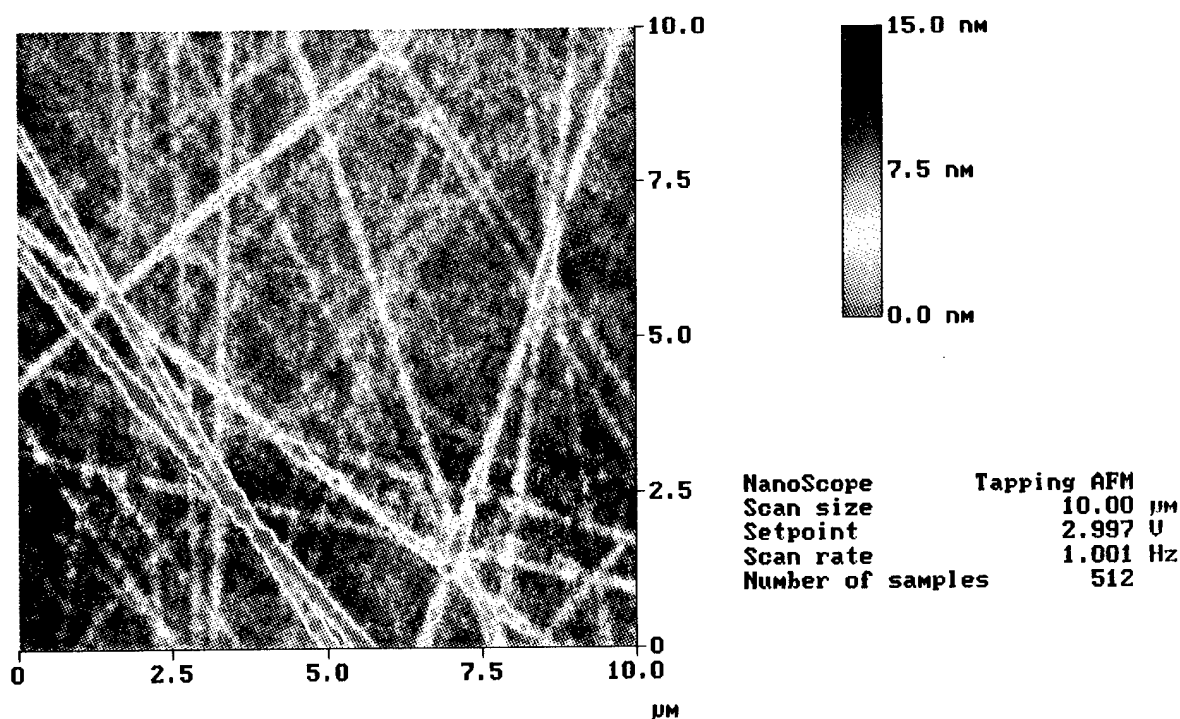
A-13 Cl<sub>2</sub>/Ar with 150 W RF power, 1000 W ECR power, 1.5 mTorr, and 0.667 active fraction.



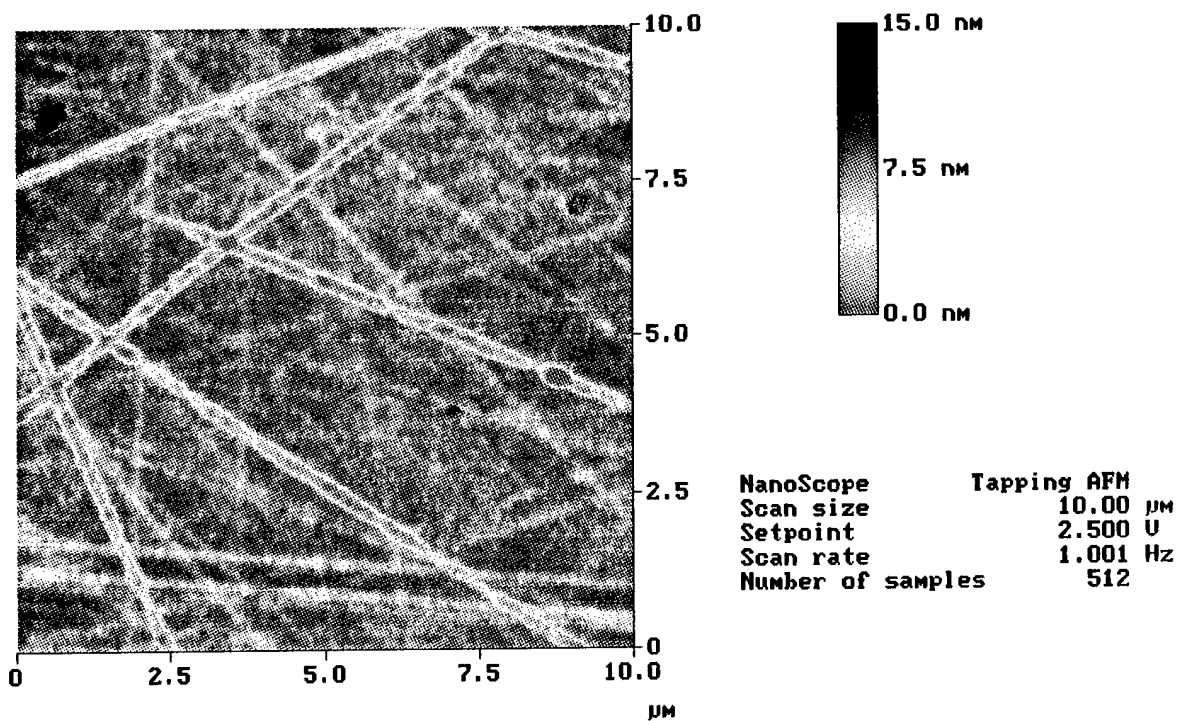
A-14 Cl<sub>2</sub>/H<sub>2</sub> with 150 W RF power, 1000 W ECR power, 1.5 mTorr, and 0.667 active fraction.



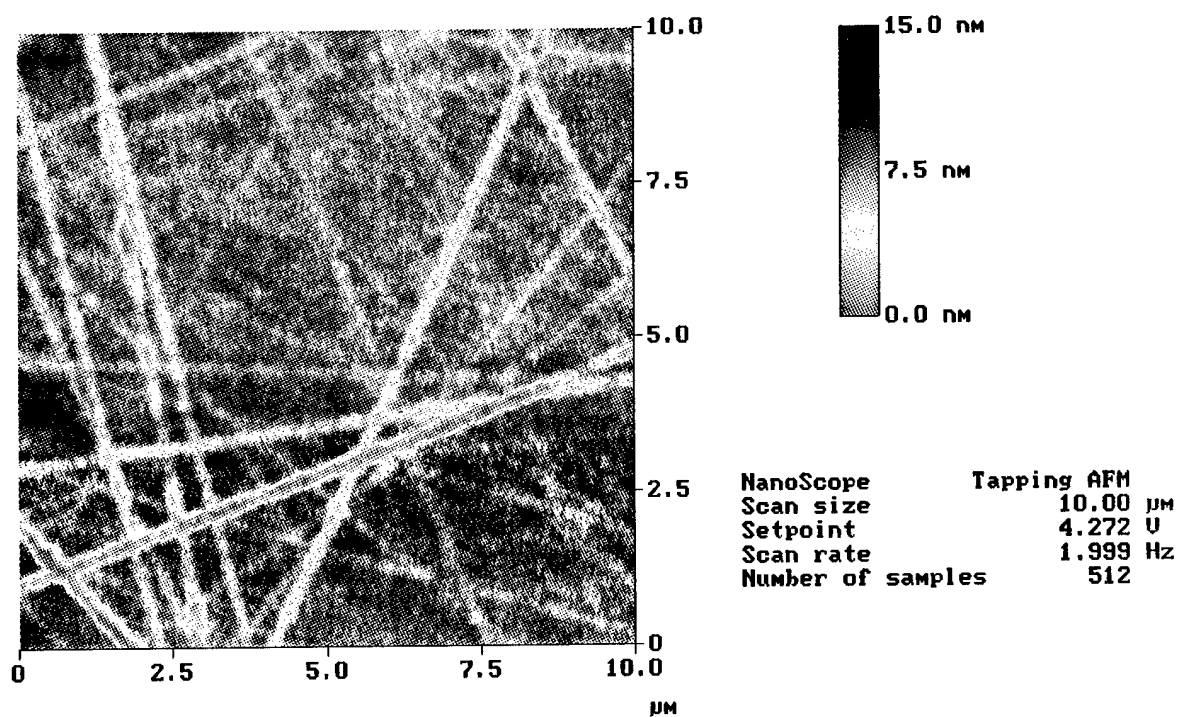
A-15 Cl<sub>2</sub>/H<sub>2</sub> with 150 W RF power, 400 W ECR power, 1.5 mTorr, and 0.667 active fraction.



A-16 Cl<sub>2</sub>/H<sub>2</sub> with 150 W RF power, 600 W ECR power, 1.5 mTorr, and 0.667 active fraction.



A-17  $\text{Cl}_2/\text{H}_2$  with 150 W RF power, 800 W ECR power, 1.5 mTorr, and 0.667 active fraction.



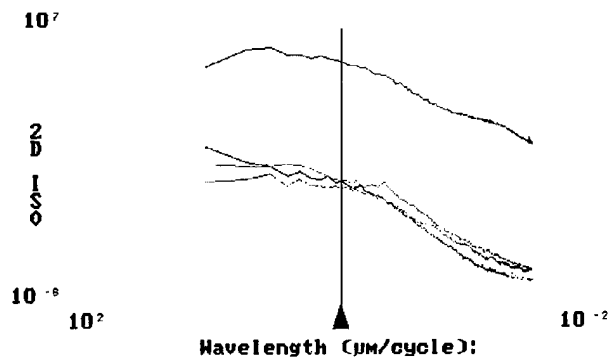
A-18  ~~$\text{Cl}_2/\text{H}_2$~~  with 150 W RF power, 800 W ECR power, 1.5 mTorr, and ~~0.667~~ active fraction.

Parent - unetched sample

**APPENDIX B**  
**POWER SPECTRAL DENSITY CURVES**

# PSD Compare

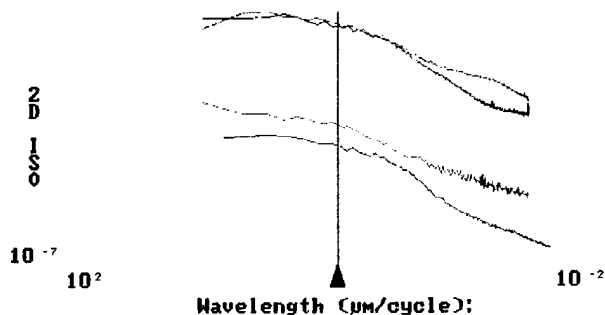
	Reference	Plot
520a	50W *	yes
521	250W	yes
522a	350W	yes
516b	150W	yes
controla		yes



	Reference				
Filename	: 520a	521	522a	516b	controla
PSD Type	: 2D	2D	2D	2D	2D
Power (nm <sup>2</sup> )	: 1.11 e-007	3.61e-007	4.44e-007	1.87e-007	0.161
1D PSD (nm <sup>3</sup> )	: 0.00111	0.00362	0.00444	0.00187	1.6e+003
1D iso PSD	: 1.68e-005	5.48e-005	6.73e-005	2.84e-005	24.4
2D iso PSD (nm <sup>4</sup> )	: 0.168	0.548	0.673	0.284	2.43e+005
Delta 2D PSD	: 0	-0.38	-0.505	-0.116	-2.43e+005
Delta Power	: 0	-2.5e-007	-3.33e-007	-7.63e-008	-0.161
Wavelength (um)	: 1				
Frequency (/um)	: 1				

B-1 PSD curves for Argon with varying RF Power.

	Reference	Plot
636a	150W *	yes
640a	50W	yes
641d	100W	yes
controla		yes
642b	250W	yes

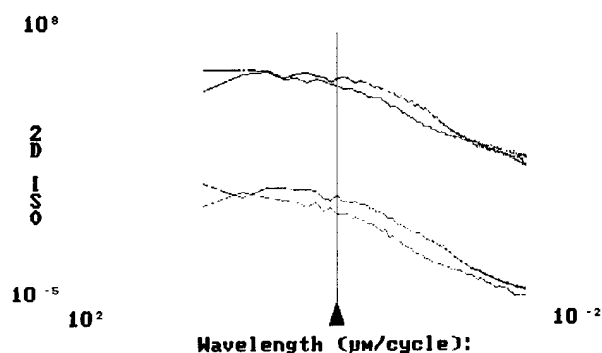


	Reference				
Filename	: 636a	640a	641d	controla	642b
PSD Type	: 2D	2D	2D	2D	2D
Power (nm <sup>2</sup> )	: 0.046	0.111	1.01e-006	0.161	1.19e-007
1D PSD (nm <sup>3</sup> )	: 460	1.1e+003	0.0101	1.6e+003	0.000824
1D iso PSD	: 6.97	16.8	0.000153	24.4	2.17e-005
2D iso PSD (nm <sup>4</sup> )	: 6.97e+004	1.67e+005	1.53	2.43e+005	0.15
Delta 2D PSD	: 0	-9.81e+004	6.96e+004	-1.74e+005	6.97e+004
Delta Power	: 0	-0.0648	0.046	-0.115	0.046
Wavelength (um)	: 1				
Frequency (/um)	: 1				

B-2 PSD curves for SF6/Ar with varying RF Power.

## PSD Compare

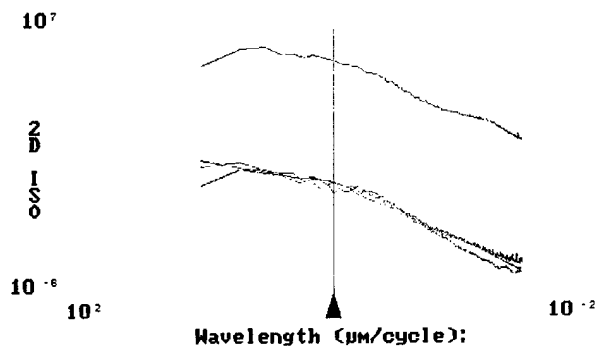
	Reference	Plot
498a	.5	yes
499a	.125	yes
500b	.25	yes
501a	1.0	yes
controla		yes



	Reference				
Filename	: 498a	499a	500b	501a	controla
PSD Type	: 2D	2D	2D	2D	2D
Power ( $\text{nm}^2$ )	: 0.853	0.363	9.76e-008	8.45e-007	0.161
1D PSD ( $\text{nm}^2$ )	: 8.53e+003	3.62e+003	0.000976	0.00845	1.6e+003
1D iso PSD	: 129	55	1.47e-005	0.000128	24.4
2D iso PSD ( $\text{nm}^2$ )	: 1.29e+006	5.49e+005	0.148	1.28	2.43e+005
Delta 2D PSD	: 0	7.42e+005	1.29e+006	1.29e+006	1.04e+006
Delta Power	: 0	0.49	0.853	0.853	0.692
Wavelength ( $\mu\text{m}$ )	: 1				
Frequency ( $/\mu\text{m}$ )	: 1				

B-3 PSD curves for IBr/Ar with varying active to total flow rate ratios.

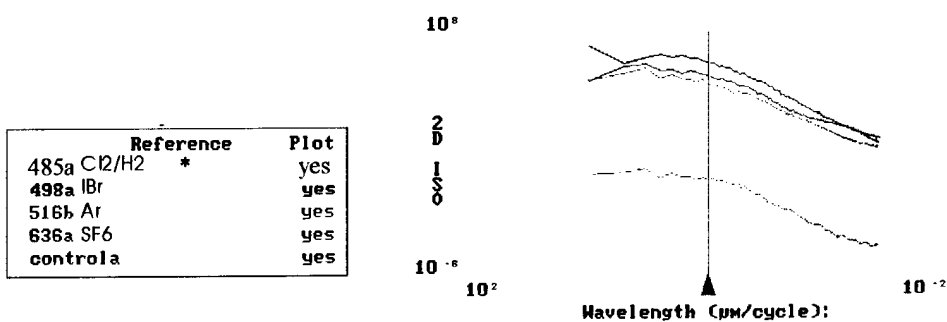
	Reference	Plot
485a	1000 W	yes
486b	800 W	yes
487a	600 W	yes
488b	400 W	yes
controla		yes



	Reference				
Filename	: 485a	486b	487a	488b	controla
PSD Type	: 2D	2D	2D	2D	2D
Power ( $\text{nm}^2$ )	: 4.48e-007	1.75e-007	1.82e-007	5.49e-008	0.161
1D PSD ( $\text{nm}^2$ )	: 0.00448	0.00175	0.00183	0.00055	1.6e+003
1D iso PSD	: 6.78e-005	2.65e-005	2.76e-005	8.33e-006	24.4
2D iso PSD ( $\text{nm}^2$ )	: 0.679	0.266	0.277	0.0833	2.43e+005
Delta 2D PSD	: 0	0.413	0.402	0.596	-2.43e+005
Delta Power	: 0	2.72e-007	2.65e-007	3.93e-007	-0.161
Wavelength ( $\mu\text{m}$ )	: 1				
Frequency ( $/\mu\text{m}$ )	: 1				

B-4 PSD curves for Cl<sub>2</sub>/H<sub>2</sub> with varying ECR Power.

## PSD Compare



	Reference				
Filename	:	485a	498a	516b	636a controla
PSD Type	:	2D	2D	2D	2D 2D
Power (nm <sup>2</sup> )	:	4.48e-007	0.853	1.87e-007	0.046 0.161
1D PSD (nm <sup>2</sup> )	:	0.00448	8.53e+003	0.00187	460 1.6e+003
1D iso PSD	:	6.78e-005	129	2.84e-005	6.97 24.4
2D iso PSD (nm <sup>4</sup> )	:	0.679	1.29e+006	0.284	6.97e+004 2.43e+005
Delta 2D PSD	:	0	-1.29e+006	0.395	-6.96e+004 -2.43e+005
Delta Power	:	0	-0.853	2.6e-007	-0.046 -0.161
Wavelength (um)	:	1			
Frequency (/um)	:	1			

B-5 PSD curves for all gas chemistries with 150 W RF, 1000 W ECR, and 1.5 mTorr.

## LIST OF REFERENCES

1. Morkoc, S. Strite, G.B. Gao, M.E. Lin, B. Sverdlov, and M. Burns. "Large-Band-Gap SiC, III-V Nitride, and II-VI ZnSe-Based Semiconductor Device Technologies." *Journal of Applied Physics*. 76 (3) 1994. pp. 1363-1371.
2. Metzger, Robert A. "Turning Blue to Green." *Compound Semiconductors*. 1 (1) 1995. pp. 26-28
3. Lande, Simon. "The Status of Silicon Carbide and Related Materials." *III-V's Review*. 9 (1) 1996. pp. 58-62.
4. Cree Research. *Properties and Specifications for 6H-Silicon Carbide*. Cree Research, Durham, NC. 1995.
5. Papanicolaou, A. Christou, and M. L. Gipe. "Pt and PtSi<sub>x</sub> Schottky Contacts on p-type  $\beta$ -SiC." *Journal of Applied Physics*. 65 (9) 1989. pp. 3526-3530.
6. Moki, A. P. Shenoy, D. Alok, and B.J. Baliga. "Low Resistivity As-Deposited Ohmic Contacts to 3C-SiC." *Journal of Electronic Materials*. 24 (4) 1995. pp. 315-317.
7. Holloway, Paul H. and Gary E. McGuire. *Handbook of Compound Semiconductors. Growth, Processing, Characterization, and Devices*. Noyles Publications. Park Ridge, NJ. 1995.
8. Wu, J and J. D. Parsons. "Reactive Ion Etching of (111)  $\beta$ -SiC Epitaxial Layers on (111) TiC Substrates in CF<sub>4</sub> + O<sub>2</sub> + Ar." *The Journal of the Electrochemical Society*. 141 (10) 1994. pp. 2915-2917.
9. Wolf, R. and R. Helbig. "Reactive Ion Etching of 6H-SiC in SF<sub>6</sub>/ O<sub>2</sub> and CF<sub>4</sub>/ O<sub>2</sub> with N<sub>2</sub> Additive for Device Fabrication." *The Journal of the Electrochemical Society*. 143 (3) 1996. pp. 1037-1042.
10. Yih, P. H. and A. J. Steckl. "Effects of Hydrogen Additive on Obtaining Residue-Free Reactive Ion Etching of  $\beta$ -SiC in Fluorinated Plasmas." *The Journal of the Electrochemical Society*. 140 (6) 1993. pp. 1813-1823.
11. Lee, J. W., S.J. Pearton, C.J. Santana, J.R. Mileham, E.S. Lambers, and C.R. Abernathy. "High Ion Density Plasma Etching of InGaP, AlInP, and AlGaP in

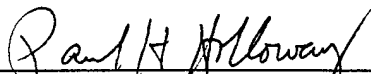


- CH<sub>4</sub>/H<sub>2</sub>/Ar.” ” *The Journal of the Electrochemical Society*. 143 (3) 1996. pp. 1093-1098.
12. Coburn, John W. *Reactive Ion Etching*. Short Course Executive Committee American Vacuum Society. Orlando, Florida. 1997.
  13. Serway, Raymond A. *Physics for Scientists and Engineers. Third Edition. Volume I*. Sanders College Publishing. Philadelphia, PN. 1990.
  14. Serway, Raymond A. *Physics for Scientists and Engineers. Third Edition. Volume II*. Sanders College Publishing. Philadelphia, PN. 1990.
  15. Lide, David R. *CRC Handbook of Chemistry and Physics*. CRC Press. Ann Arbor, MI. 1991-1992.


## BIOGRAPHICAL SKETCH

Gavin McDaniel was born on April 03, 1973, in Greenville, South Carolina. He attended Spartanburg High School in Spartanburg, South Carolina, and graduated in May of 1991. He went directly to The United States Air Force Academy in Colorado Springs where he received a dual bachelor's degree in chemistry and applied physics. He graduated in the top 18% of his class and was commissioned as a second lieutenant on May 31, 1995. Under an Air Force Institute of Technology fellowship, he went directly to the University of Florida to pursue a master's degree in materials science and engineering, where he worked as a graduate assistant under the direction of Dr. Paul H. Holloway and Dr. Stephen Pearton. During his work at the university, he has pursued two additional degrees to include a minor in electrical engineering and a Ph.D. in materials science and engineering. He plans to receive his master of science degree in materials engineering and his minor in electrical engineering in May of 1997. Afterward, he will report to Wright Patterson Air Force Base and under the direction of Dr. Bill Lampert to continue semiconductor studies. He plans to complete his doctor of philosophy in materials engineering nonresident from the University of Florida while on active duty at the Wright Laboratories.

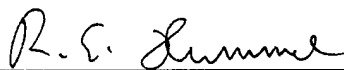
I certify that I have read this study and that in my opinion it conforms to acceptable standards of scholarly presentation and is fully adequate, in scope and quality, as a thesis for the degree of Master of Science.

  
Paul H. Holloway, Chairman  
Professor of Materials Science and  
Engineering

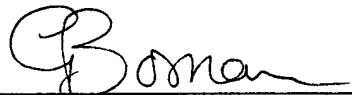
I certify that I have read this study and that in my opinion it conforms to acceptable standards of scholarly presentation and is fully adequate, in scope and quality, as a thesis for the degree of Master of Science.

  
Stephen J. Pearton  
Professor of Materials Science and  
Engineering

I certify that I have read this study and that in my opinion it conforms to acceptable standards of scholarly presentation and is fully adequate, in scope and quality, as a thesis for the degree of Master of Science.

  
Rolf E. Hummel  
Professor of Materials Science and  
Engineering

I certify that I have read this study and that in my opinion it conforms to acceptable standards of scholarly presentation and is fully adequate, in scope and quality, as a thesis for the degree of Master of Science.

  
Gijs Bosman  
Professor of Electrical and Computer  
Engineering

This thesis was submitted to the Graduate Faculty of the College of Engineering and to the Graduate School and was accepted as partial fulfillment of the requirements for the degree of Master of Science.

May 1997

\_\_\_\_\_  
Winfred M. Phillips  
Dean, College of Engineering

\_\_\_\_\_  
Karen A. Holbrook  
Dean, Graduate School